

Chapter 2

Nuclear Reactor Calculations

Keisuke Okumura, Yoshiaki Oka, and Yuki Ishiwatari

Abstract The most fundamental evaluation quantity of the nuclear design calculation is the effective multiplication factor (k_{eff}) and neutron flux distribution. The excess reactivity, control rod worth, reactivity coefficient, power distribution, etc. are undoubtedly inseparable from the nuclear design calculation. Some quantities among them can be derived by secondary calculations from the effective multiplication factor or neutron flux distribution. Section 2.1 treats the theory and mechanism to calculate the effective multiplication factor and neutron flux distribution in calculation programs (called *codes*). It is written by Keisuke Okumura.

The nuclear reactor calculation is classified broadly into the reactor core calculation and the nuclear plant characteristics calculation. The former is done to clarify nuclear, thermal, or their composite properties. The latter is done to clarify dynamic and control properties, startup and stability, and safety by modeling pipes and valves of the coolant system, coolant pump, their control system, steam turbine and condenser, etc. connected with the reactor pressure vessel as well as the reactor core. The reactor core, plant dynamics, safety analysis and fuel rod analysis are described in Sect. 2.2. It is written by Yoshiaki Oka and Yuki Ishiwatari.

2.1 Nuclear Design Calculations

2.1.1 Fundamental Neutron Transport Equation

The collective behavior of neutrons in a reactor core is described by the neutron transport equation presented in Eq. (2.1) which is also referred to as the Boltzmann equation.

$$\frac{1}{v} \frac{\partial}{\partial t} \phi(\vec{r}, \vec{\Omega}, E, t) = S(\vec{r}, \vec{\Omega}, E, t) - \vec{\Omega} \cdot \nabla \phi(\vec{r}, \vec{\Omega}, E, t) - \Sigma_t(\vec{r}, E, t) \phi(\vec{r}, \vec{\Omega}, E, t) \quad (2.1)$$

Here, S is the neutron source, Σ_t is the macroscopic total cross section, and ϕ is the angular neutron flux being calculated. This equation represents the balance between gain and loss in the unit volume of neutrons that are characterized by a specific kinetic energy E (velocity v) and are traveling in a specific direction $\vec{\Omega}$ at a time t and a position \vec{r} . That is, the time change of the target neutrons (the first term in the LHS) is given by the balanced relation among: the gain of neutrons appearing from the neutron source S (the first in the RHS), the net loss of neutrons traveling (the second term in the RHS), and the loss of neutrons due to nuclear collisions (the third term in the RHS). It should be noted that the changes in angle and energy of neutrons are also included in the gain and loss.

The target neutrons are gained from three mechanisms: scattering, fission, and external neutron sources. Each gain is represented in

$$\begin{aligned} S(\vec{r}, \vec{\Omega}, E, t) = & \int_0^\infty dE' \int_{4\pi} \Sigma_s(\vec{r}, \vec{\Omega}' \rightarrow \vec{\Omega}, E' \rightarrow E, t) \phi(\vec{r}, \vec{\Omega}', E', t) d\Omega' \\ & + \frac{\chi(E)}{4\pi} \int_0^\infty dE' \int_{4\pi} \chi(E) v \Sigma_f(\vec{r}, E', t) \phi(\vec{r}, \vec{\Omega}', E', t) d\Omega' \\ & + S_{ex}(\vec{r}, \vec{\Omega}, E, t) \end{aligned} \quad (2.2)$$

where Σ_s and Σ_f are the macroscopic scattering and fission cross sections, respectively. v is the average number of neutrons released per fission and the product $v\Sigma_f$ is treated as a production cross section. The cross sections are described in the next section.

The first term in the RHS of Eq. (2.2) is called the *scattering source* and it totals the number of the target neutrons scattering into E and $\vec{\Omega}$ from another energy E' and direction $\vec{\Omega}'$ by integrating the number for E' and $\vec{\Omega}'$. The second term is the fission source and it indicates that the neutrons produced by fission over the whole range of energies are distributed with the isotropic probability in direction ($1/4\pi$) and the probability $\chi(E)$ in energy. $\chi(E)$ is called the *fission spectrum* and it is dependent on the nuclide undergoing fission and the energy of incident neutrons. For instance, the fission spectrum in an enriched uranium-fueled LWR is well described by the function of Eq. (2.3).

$$\chi(E) = \sinh \sqrt{2.29E} \exp(-E/0.965) \quad (2.3)$$

Since $\chi(E)$ is a probability distribution function, it is normalized so that

$$\int_0^\infty \chi(E) dE = 1.0 \quad (2.4)$$

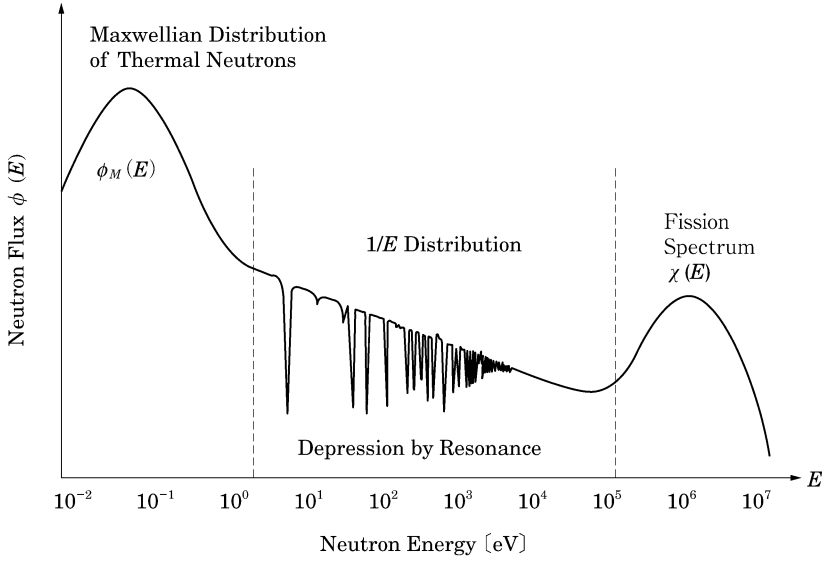


Fig. 2.1 Neutron spectrum of a thermal reactor

The third term in the RHS of Eq. (2.2), S_{ex} , expresses the external neutron source for reactor startup which may be such species as ^{252}Cf or Am-Be. Therefore, it is not used in the nuclear design calculation of a reactor in operation.

More details of the neutron transport equation are not handled here. If the cross section data (Σ_t , Σ_s , and $\nu\Sigma_f$) in Eqs. (2.1) and (2.2) are provided, the angular neutron flux $\phi(\vec{r}, \vec{\Omega}, E, t)$, which depends on location, traveling direction, energy, and time, can be calculated by properly solving the equation.

The information on traveling direction of neutrons is finally unimportant in the nuclear design calculation. The scalar neutron flux integrated over the angle is rather meaningful.

$$\phi(\vec{r}, E, t) = \int_0^{4\pi} \phi(\vec{r}, \vec{\Omega}, E, t) d\Omega \quad (2.5)$$

2.1.2 Neutron Spectrum

The function characterizing the energy dependence of neutron flux $\phi(\vec{r}, E, t)$ is called the *neutron spectrum* and it varies with fuel enrichment, moderator density, void fraction, burnup, and so on. Figure 2.1 shows a neutron spectrum of a thermal reactor. The neutron spectrum of thermal reactors is divided into three distinct energy regions. In the high-energy region above 10^5 eV, since the prompt neutrons released by fission are dominant, the neutron spectrum is approximately

proportional to the fission spectrum $\chi(E)$. In the energy region below several hundred of keV, the fast neutrons from fission lose their energies mainly through elastic scattering reaction with light moderator nuclides such as hydrogen.

According to neutron slowing-down theory [1], when fast neutron sources are in an infinite homogeneous medium which is an ideal moderator with negligible absorption, the neutron energy spectrum behaves as $1/E$.

$$\phi(E) \propto \frac{1}{E} \quad (2.6)$$

In the practical medium of fuel and moderator, the $1/E$ distribution is characterized by the occurrence of fairly sharp depressions due to the resonance absorption of ^{238}U , etc. as shown in Fig. 2.1. Moreover, if the resonance absorption is large, the neutron flux becomes somewhat smaller than the $1/E$ distribution in the low energy region.

If neutrons are moderated below several eV of kinetic energy, the kinetic energy by thermal vibration of nuclei cannot be ignored. In other words, if the kinetic energies of neutrons become appropriately small, the neutrons collide with thermally vibrating moderator nuclei and their kinetic energies become reversely large. This is called *up-scattering* against moderation (*down-scattering*). In this energy region, the neutron spectrum is characterized in a thermal equilibrium at a temperature T by a balance between down-scattering and up-scattering. Further, in the ideal infinite medium without absorption, the thermal equilibrium neutron spectrum is described by the following Maxwellian distribution function

$$\phi_M(E) \propto E \cdot \exp\left(-\frac{E}{kT}\right) \quad (2.7)$$

where k is the Boltzmann constant. At room temperature ($T = 300 \text{ K}$), ϕ_M is maximized at $E = 0.0253 \text{ eV}$ for which the corresponding velocity is $2,200 \text{ m/s}$.

On being absorbed, the thermal neutron spectrum deviates a little from $\phi_M(E)$ forward the high energy region because absorption cross sections are larger in lower energies. This is called *absorption hardening*. To compensate the Maxwellian distribution for the absorption hardening, neutron temperature, which is a little higher than moderator temperature, is used as T of Eq. (2.7).

2.1.3 Nuclear Data and Cross Sections

[1] Macroscopic cross sections

The cross section used in the neutron transport equation, Σ , is called the macroscopic cross section and its unit is (cm^{-1}) . The macroscopic cross section of nuclear reaction x is the sum of the product of atomic number density N^i and microscopic cross section σ_x^i of a constituent nuclide i of the material at a position \vec{r} . It is expressed as Eq. (2.8).

Table 2.1 Classification of key nuclear reactions in nuclear reactors

Classification	Reaction	Transcription	Cross section symbol	Reaction example
Scattering (σ_s)	Elastic scattering	(n, n)	σ_e	$^1\text{H}(n, n)$
	Inelastic scattering	(n, n')	σ_{in}	$^{238}\text{U}(n, n')$
Absorption (σ_a)	Radiative capture	(n, γ)	σ_γ	$^{238}\text{U}(n, \gamma)$
	Fission	(n, f)	σ_f	$^{235}\text{U}(n, f)$
	Charged-particle emission	(n, p) (n, α)	σ_p σ_α	$^{14}\text{N}(n, p)$ $^{10}\text{B}(n, \alpha)$
	Neutron emission	$(n, 2n)^a$	$\sigma_{(n, 2n)}$	$^9\text{Be}(n, 2n)$

^aThe $(n, 2n)$ reaction can be treated as a special scattering reaction. Here this reaction, which transmutes the nuclide, is classified as an absorption reaction

$$\Sigma_x(\vec{r}, E, t) = \sum_i N^i(\vec{r}, t) \sigma_x^i(E) \quad (2.8)$$

The atomic number density N^i can be given by

$$N^i(\vec{r}, t) = \frac{\rho^i(\vec{r}, t)}{M^i} N_A \quad (2.9)$$

where ρ^i is the density occupied by i in the material, M^i is the atomic mass, and N_A is Avogadro's number. Variation of atomic number density with position and time should be considered in power reactors, reflecting fuel burnup or coolant void fraction.

[2] Microscopic cross sections

Interactions between neutrons and nuclei in nuclear reactors can be classified broadly into scattering and absorption reactions as shown in Table 2.1. Scattering is further classified into elastic scattering in which the kinetic energy is conserved before and after the reaction, and inelastic scattering in which a part of the kinetic energy is used in exciting a target nucleus. In absorption, the main reactions are capture, fission, charged-particle emission, and neutron emission. Thus, the microscopic cross sections of the total, scattering, and absorption reactions are given by

$$\text{total cross section: } \sigma_t(E) = \sigma_s(E) + \sigma_a(E) \quad (2.10)$$

$$\text{scattering cross section: } \sigma_s(E) = \sigma_e(E) + \sigma_{in}(E) \quad (2.11)$$

$$\begin{aligned} \text{absorption cross section:} \\ \sigma_a(E) = \sigma_\gamma(E) + \sigma_f(E) + \sigma_p(E) + \sigma_\alpha(E) + \sigma_{(n, 2n)}(E) \end{aligned} \quad (2.12)$$

It is useful to discuss a general energy dependence of these microscopic cross sections. The neutron energy range to be considered in design of nuclear reactors is from the Maxwellian distribution of the thermal neutrons at room temperature to the fission spectrum of the prompt neutrons. Most nuclear design codes handle the range of 10^{-5} eV–10 MeV. In this energy range, the

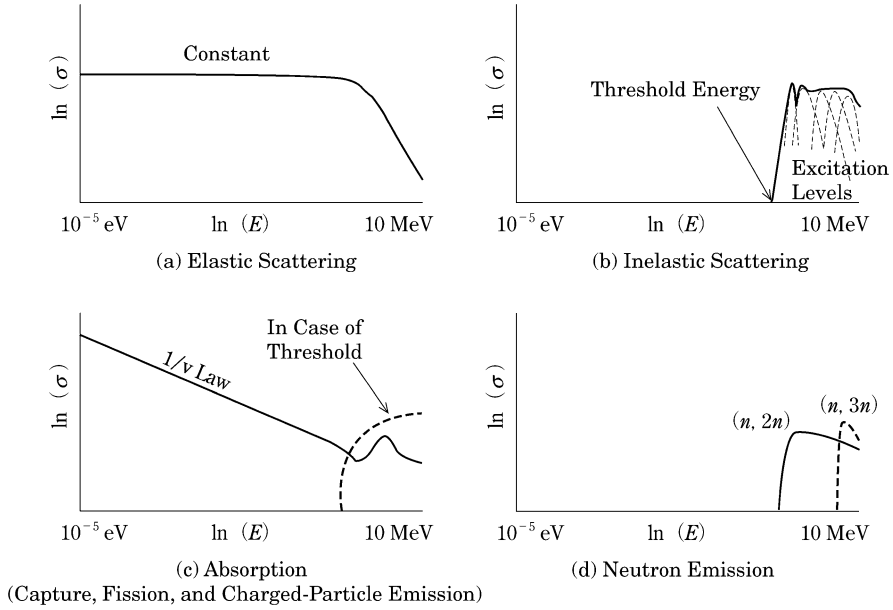


Fig. 2.2 Energy dependence of cross sections

microscopic cross sections introduced in Eqs. (2.10), (2.11), and (2.12) behave as shown in Fig. 2.2.

The elastic scattering cross section is mostly constant in all the energies except for the MeV region. Meanwhile, in inelastic scattering, the incident neutron should have sufficient kinetic energy to place the target nucleus in its excited state. Hence, the inelastic scattering cross section is zero up to some threshold energy of several MeV. Fast neutrons can be moderated by inelastic scattering with heavy nuclides, but by elastic scattering with light nuclides below threshold energies of the heavy nuclides.

Most absorption cross sections including the fission cross section appear as a straight line with a slope of $-1/2$ on a log-log scale. This means that the absorption cross sections are inversely proportional to the neutron speed ($1/v$ law) and therefore increase as the neutron energy decreases. Using such large fission cross sections at low neutron energies and thermal neutrons in the Maxwellian distribution make it possible that natural or low-enrichment uranium fueled reactors reach a critical state. The current thermal reactors, represented by LWRs, use the characteristics of the cross section.

For heavy nuclides such as fuel materials, many resonances are observed in elastic scattering and absorption cross section as shown in Fig. 2.3. The widths of the resonances broaden as fuel temperature increases. This is called the *Doppler effect*. The width broadening facilitates resonance absorption of neutrons under moderation. Most low-enrichment uranium fuel is composed of

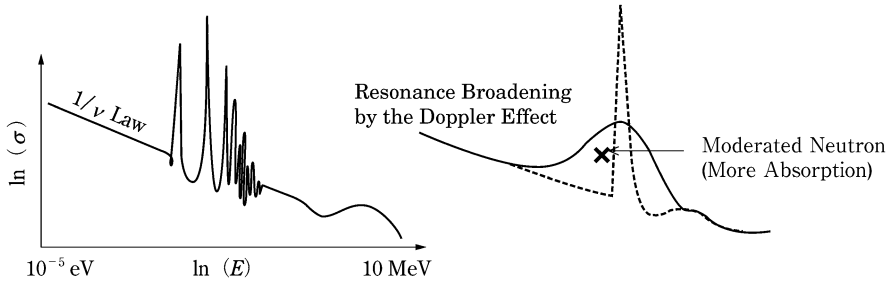


Fig. 2.3 Resonance absorption cross section and Doppler effect

fertile ^{238}U and thermal neutrons escaping from the resonance of capture reaction induce fissions for the next generation.

Hence, a rise in fuel temperature leads to a decrease in resonance escape probability of moderated neutrons and then fission events in the reactor decrease with thermal neutrons. Such a mechanism is called *negative temperature feedback*. The temperature dependence is not described in the Boltzmann equation of Eq. (2.1), but reflected in the cross sections of the equation.

[3] Evaluated nuclear data file

The primal data (microscopic cross sections, etc.) for the nuclear reactor calculation are stored in the evaluated nuclear data file which includes cross sections uniquely-determined in the whole range of neutron energy on the basis of fragmentally measured and/or theoretically calculated parameters. The cross sections are given for all possible nuclear reactions of more than 400 nuclides. JENDL [2], ENDF/B [3], and JEFF [4] are representative evaluated nuclear data files.

Extensive data are stored in 80-column text format in the evaluated nuclear data file as shown in Fig. 2.4 and complicated data such as resonance cross sections are also compactly-represented by mathematical formulas and their parameters.

The evaluated nuclear data, from anywhere in the world, are described based on the same format which might not make sense to beginners. The format has been changed according to advances in nuclear data and the current latest format is called ENDF-6 [5]. Various data of delayed neutron fractions, fission yields, half-lives, etc. as well as cross sections are available.

[4] Multi-group cross sections

The cross sections stored in the evaluated nuclear data file are continuous-energy data, which are converted to multi-group cross sections through energy discretization in formats suitable for most of nuclear design calculation codes, as shown in Fig. 2.5. The number of energy groups (N) is dependent on nuclear design codes and is generally within 50–200.

Multi-group cross sections are defined that integral reaction rates for reactions ($x = s, a, f, \dots$) of a target nuclide i) should be conserved within the range

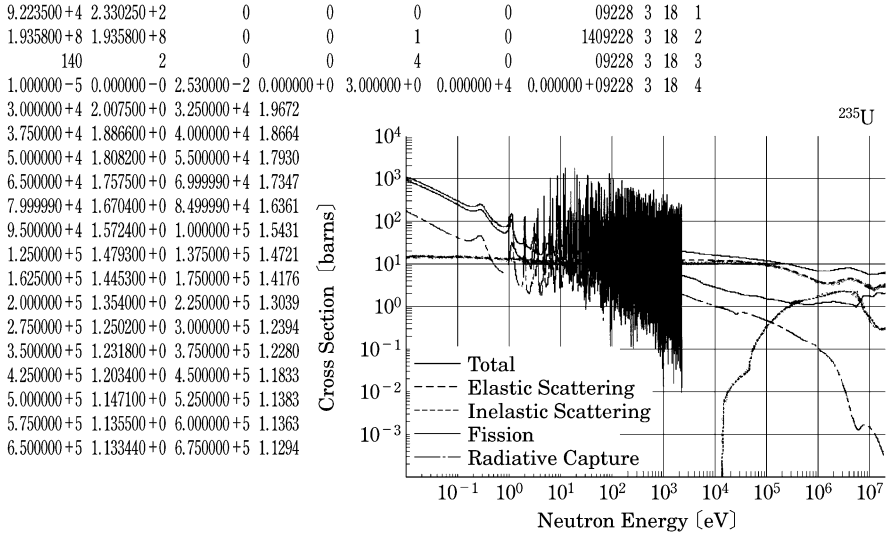


Fig. 2.4 Example of ^{235}U cross sections stored in JENDL (Right bottom figure: plot of the cross sections)

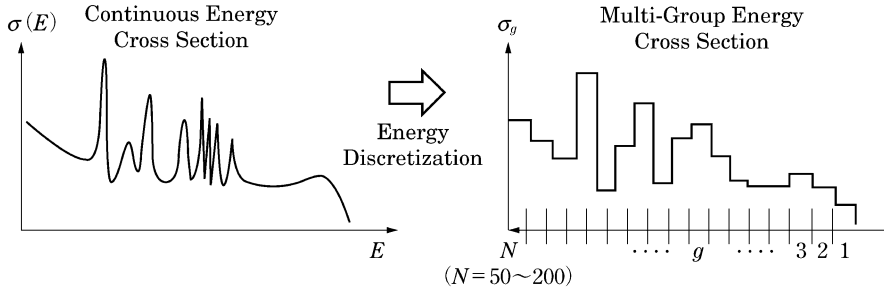


Fig. 2.5 Multi-group cross section by energy discretization

of energy group g (ΔE_g), as shown in Eq. (2.13). The neutron flux and cross section in group g are defined as Eqs. (2.14) and (2.15), respectively.

$$\int_{\Delta E_g} \sigma_x^i(E) \phi(E) dE = \sigma_{x,g}^i \phi_g \quad (2.13)$$

$$\phi_g \equiv \int_{\Delta E_g} \phi(E) dE \quad (2.14)$$

$$\sigma_{x,g}^i \equiv \frac{\int_{\Delta E_g} \sigma_x^i(E) \phi(E) dE}{\int_{\Delta E_g} \phi(E) dE} \quad (2.15)$$

The neutron spectrum of Fig. 2.1 can be used as $\phi(E)$ in Eq. (2.15) for thermal reactors. However, while those multi-group cross sections are introduced to calculate neutron flux in reactors, it is apparent that the neutron flux is necessary to define the multi-group cross sections. This is recursive and contradictory. For example, the depression of neutron flux due to resonance, shown in the $1/E$ region of Fig. 2.1, depends on fuel composition (concentrations of resonance nuclides) and temperature (the Doppler effect). It is hard to accurately estimate the neutron flux before design calculation. In actual practice, consideration is made for a representative neutron spectrum ($\phi_w(E)$: called the “weighting spectrum”) which is not affected by the resonance causing the depression and is also independent of position. Applying it to Eq. (2.15) gives Eq. (2.16).

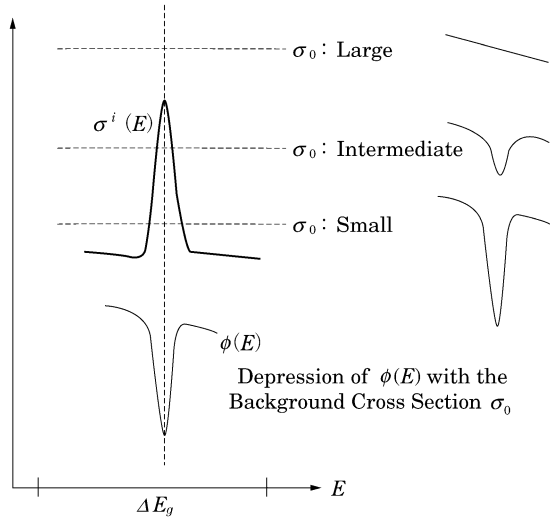
$$\sigma_{\infty, x, g}^i \equiv \frac{\int_{\Delta E_g} \sigma_x^i(E) \phi_w(E) dE}{\int_{\Delta E_g} \phi_w(E) dE} \quad (2.16)$$

Since these microscopic cross sections are not concerned with detailed design specifications of fuel and operating conditions of the reactor, it is possible to prepare them beforehand using the evaluated nuclear data file. The depression or distortion of neutron flux does not occur for resonance nuclides at sufficiently dilute concentrations and this is called the *infinite dilution cross section* ($\sigma_{\infty, x, g}^i$). On the other hand, the cross section prepared in Eq. (2.15) compensates for the neutron spectrum depression due to resonance in the $1/E$ region by some method, and is called the “effective (microscopic) cross section” ($\sigma_{eff, x, g}^i$). There are several approximation methods for the effective resonance cross section: NR approximation, WR approximation, NRIM approximation, and IR approximation. For more details, references [1, 6] on reactor physics should be consulted. The relationship between the effective cross section and infinite dilution cross section is simply discussed here.

Since neutron mean free path is long in the resonance energy region, a homogenized mixture of fuel and moderator nuclides, ignoring detailed structure of the materials, can be considered. If a target nuclide (i) in the mixture has a resonance, it leads to a depression in the neutron flux at the corresponding resonance energy as shown in Fig. 2.6. The reaction rate in the energy group including the resonance becomes smaller than that in the case of no flux depression (infinite dilution). Hence, the effective cross section is generally smaller than its infinite dilution cross section. The following definition is the ratio of the effective cross section to the infinite dilution cross section and called the *self-shielding factor*.

$$f_{x, g}^i \equiv \frac{\sigma_{eff, x, g}^i}{\sigma_{\infty, x, g}^i} \quad (2.17)$$

Fig. 2.6 Neutron flux depression in resonance



In Fig. 2.6, the neutron flux depression becomes large as the macroscopic cross section ($N_i\sigma_i$) of the target nuclide becomes large. On the other hand, if the macroscopic total cross section ($\sum_{j \neq i} N^j \sigma_t^j$) of other nuclides (assuming that they have no resonance at the same energy) becomes large, the resonance cross section of the target nuclide is buried in the total cross section of other nuclides and then the flux depression finally disappears when the total cross section is large enough. To treat this effect quantitatively, a virtual cross section (the *background cross section*) of the target nuclide, converted from the macroscopic total cross section, is defined as Eq. (2.18).

$$\sigma_0^i \equiv \sum_{j \neq i} N^j \sigma_t^j / N^i \quad (2.18)$$

The self-shielding factor is dependent on the background cross section and the temperature of resonance material because the resonance width varies with the Doppler effect. In fact, the background cross section and material temperature are unknown before design specifications and operating conditions of a reactor are determined. Hence, self-shielding factors are calculated in advance and tabulated at combinations of representative background cross sections and temperatures. Figure 2.7 shows a part of the self-shielding factor table (f table) for the capture cross section of ^{238}U . The self-shielding factor in design calculation is interpolated from the f table at a practical background cross section (σ_0) and temperature (T). The effective microscopic cross section for neutron transport calculation can be obtained from the self-shielding factor as

$$\sigma_{eff, x, g}^i(\sigma_0, T) = f_{x, g}^i(\sigma_0, T_0 \rightarrow T) \cdot \sigma_{\infty, x, g}^i(T_0) \quad (2.19)$$

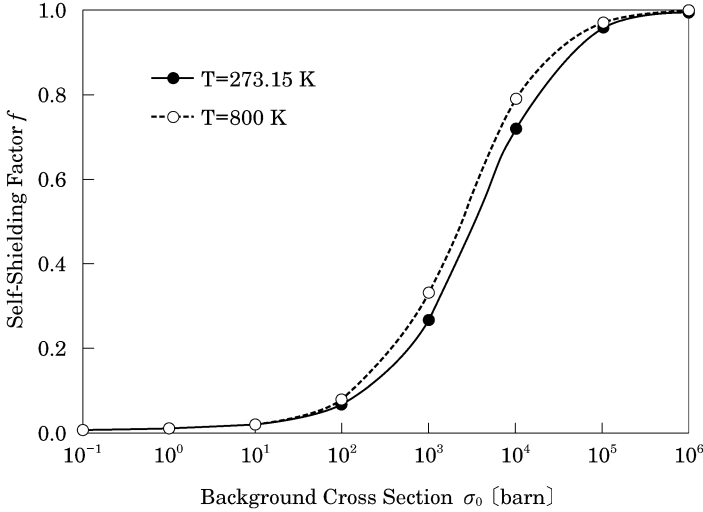


Fig. 2.7 Self-shielding factor of ^{238}U capture cross section ($\Delta E_g = 6.48 \sim 8.32$ eV)

where T_0 is normally 300 K as a reference temperature at which the multi-group infinite dilution cross sections are prepared from the evaluated nuclear data file.

Recent remarkable advances in computers have made it possible that continuous-energy data or their equivalent ultra-fine-groups (groups of several tens of thousands to several millions) are employed in solving the neutron slowing-down equation and the effective cross sections of resonance nuclides are directly calculated based on Eq. (2.15). Some open codes, SRAC [7] (using the PEACO option) and SLAROM-UF [8] for fast reactors, adopt this method. This method can result in a high accuracy for treating even interference effects of multiple resonances which cannot be considered by the interpolation method of a self-shielding factor table, though a long calculation time is required for a complicated system.

[5] Nuclear data processing and reactor constant library

Nuclear design codes do not use all the massive information contained in the evaluated nuclear data file and also cannot always effectively read out necessary data because of the data format putting weight on the compact storage. Therefore, nuclear design codes do not directly read out the evaluated nuclear data file, but (i) extract necessary data and (ii) prepare a preprocessed data set (reactor constant library) which is one processed suitably for each code. A series of tasks is done in order, for example, to select nuclides and cross section data required for nuclear design, to prepare their infinite dilution cross sections and self-shielding factor tables for a specified energy group structure of a nuclear design code, and to store the data in a quickly accessible form. As nuclear data processing code systems to perform such work, NJOY [9] of LANL and PREPRO [10] of IAEA have been used all over the world.

There are two different forms of the reactor constant library; a continuous-energy form and a multi-group energy form. The former is used in continuous-energy Monte Carlo codes such as MCNP [11] and MVP [12] and the latter in nuclear design codes.

Since most nuclear design codes are provided as a set with a multi-group reactor constant library, it is usually unnecessary to process the evaluated nuclear data file in the nuclear design. However, when introducing the latest evaluated nuclear data file or changing the energy group structure to meet advances in fuel and design specification of nuclear reactors, a new reactor constant library is prepared using the nuclear data processing code system. The reactor constant library, with which a nuclear design calculation begins, might be regarded as a general-purpose library. However, it should be noted that a weighting spectrum specified in part for a reactor type and resonance approximations are employed in preparing a multi-group form library.

Nuclear characteristic calculation methods depend on the type of reactor being targeted. The following discussions center on LWR (especially BWR) calculation methods which need the most considerations such as heterogeneity of the fuel assembly, effects of the nuclear and thermal-hydraulic coupled core calculation, and so on.

2.1.4 Lattice Calculation

[1] Purpose of lattice calculation

Even using a high performance computer, a direct core calculation with several tens of thousands of fuel pins is difficult to perform in its heterogeneous geometry model form, using fine-groups (e.g., 107 groups in SRAC) of a prepared reactor constant library. The Monte Carlo method can handle such a core calculation, but it is not easy to obtain enough accuracy for a local calculation or small reactivity because of accompanying statistical errors. Hence, the Monte Carlo method is not employed for nuclear design calculations requiring a fast calculation time. Instead, the nuclear design calculation is performed in two steps: lattice calculation in a two-dimensional (2D) infinite arrangement of fuel rods or assemblies and core calculation in a three-dimensional (3D) whole core. The lattice calculation prepares few-group homogenized cross sections which maintain the important energy dependence (neutron spectrum) of nuclear reactions, as shown in Fig. 2.8, and this reduces the core calculation cost in terms of time and memory. Since final design parameters in the core calculation are not concerned with the energy dependence, the spatial dependence such as for the power distribution is important.

[2] Multi-group neutron transport equation

The neutron transport equation in the lattice calculation is a steady-state equation without the time differential term in Eq. (2.1). Further, the neutron energy variable is discretized in the equation and therefore a multi-group form

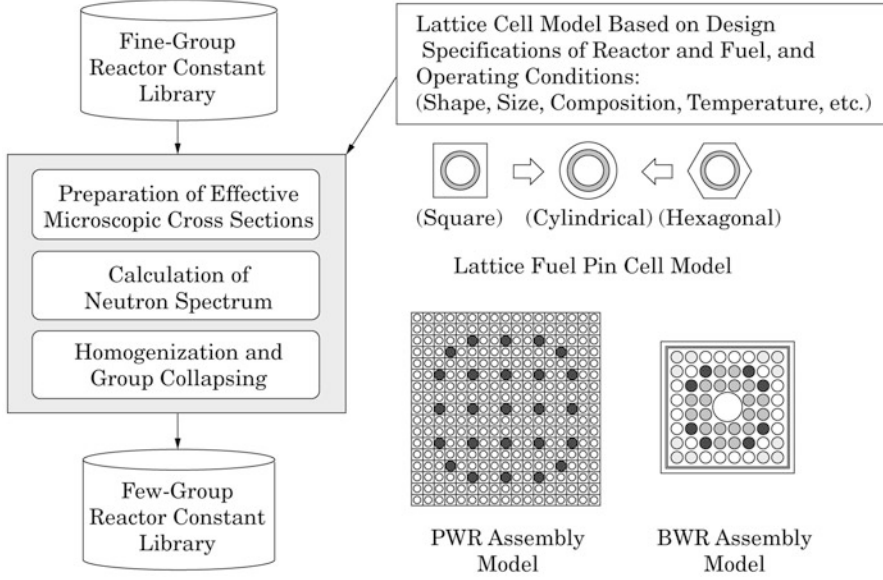


Fig. 2.8 Lattice calculation flow

is used in design codes as shown in Eq. (2.20). The neutron source of Eq. (2.21) is the multi-group form without the external neutron source of Eq. (2.2) at the critical condition.

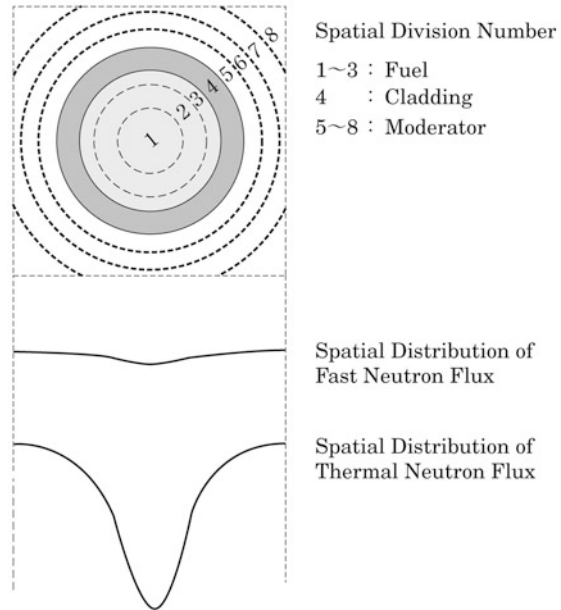
$$-\vec{\Omega} \cdot \nabla \phi_g(\vec{r}, \vec{\Omega}) - \Sigma_{t,g}(\vec{r}) \phi_g(\vec{r}, \vec{\Omega}) + S_g(\vec{r}, \vec{\Omega}) = 0 \quad (2.20)$$

$$S_g(\vec{r}, \vec{\Omega}) = \int_{4\pi} d\Omega' \sum_g \Sigma_{s,g' \rightarrow g}(\vec{r}, \vec{\Omega}' \rightarrow \vec{\Omega}) \phi_{g'}(\vec{r}, \vec{\Omega}') + \frac{\chi_g}{4\pi} \sum_g \nu \Sigma_{f,g'}(\vec{r}) \int_{4\pi} \phi_{g'}(\vec{r}, \vec{\Omega}') d\Omega' \quad (2.21)$$

The system to which the multi-group transport equation is applied is an infinite lattice system of a 2D fuel assembly (including assembly gap) with a reflective boundary condition. For a complicated geometry, two lattice calculations corresponding to a single fuel rod and a fuel assembly are often combined.

In practically solving Eq. (2.20) in the lattice model, the space variable (\vec{r}) is also discretized in the equation and each material region is divided into several sub-regions where neutron flux is regarded to be flat. In liquid metal-cooled fast reactors (LMFRs), neutron flux in each energy group has an almost flat spatial distribution within the fuel assembly because the mean free path of the fast neutrons is long. A simple hexagonal lattice model covering a single fuel rod or its equivalent cylindrical model simplified to one dimension is used in the

Fig. 2.9 Example of spatial division in rectangular lattice model of LWRs



design calculation of LMFRs. The spatial division can also be simplified by assigning the macroscopic cross section by material.

On the other hand, thermal reactors have a highly non-uniform distribution (called the *spatial self-shielding effect*) of neutron flux in a fuel assembly as thermal neutron flux rises in the moderator region or steeply falls in the fuel and absorber as shown in Fig. 2.9. Moreover, control rod guide tubes or water rods are situated within fuel assemblies and differently enriched fuels or burnable poison (Gd_2O_3) fuels are loaded. In such a lattice calculation, therefore, it is necessary to make an appropriate spatial division in the input data predicting spatial distribution of thermal neutron flux and its changes with burnup.

Numerical methods of Eq. (2.20) include the collision probability method (CPM), the current coupling collision probability (CCCP) method, and the method of characteristics (MOC) [13]. The SRAC code adopts the collision probability method and can treat the geometrical models as shown in Fig. 2.10. The collision probability method has been widely used in the lattice calculation, but it has a disadvantage that a large number of spatial regions considerably raise the computing cost. The current coupling collision probability method applies the collision probability method to the inside of fuel rod lattices constituting a fuel assembly and combines neighboring fuel rod lattices by neutron currents entering and leaving the lattices. This approach can substantially reduce the assembly calculation cost. Since the method of characteristics solves the neutron transport equation along neutron tracks, it provides computations at relatively low cost even for complicated geometrical shapes and it has become the mainstream in the recent assembly calculation [14].

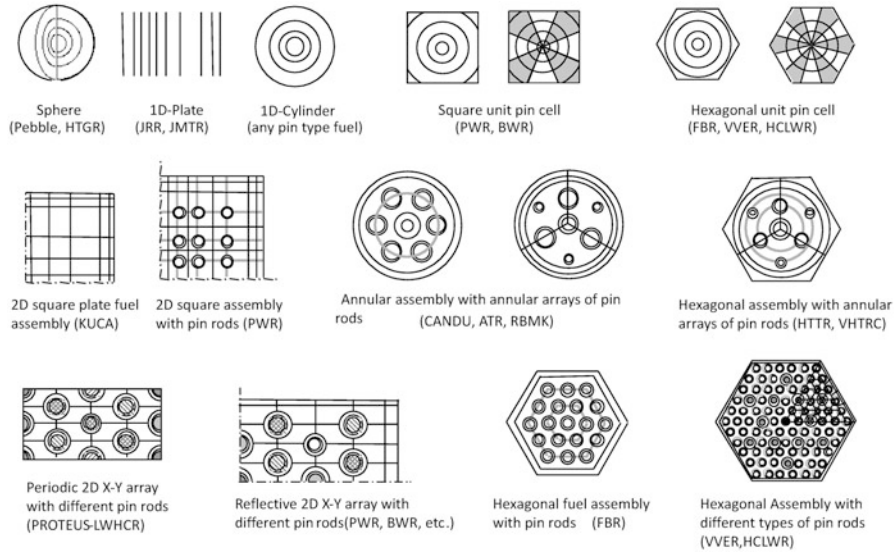


Fig. 2.10 Lattice models of SRAC [7]

In lattice calculation codes, effective microscopic cross sections are first prepared from fine-group infinite dilution cross sections based on input data such as material compositions, dimensions, temperatures, and so on. The effective cross sections are provided in solving Eqs. (2.20) and (2.21) by the use of the collision probability method, etc. and then multi-group neutron spectra are obtained in each divided region (neutron spectrum calculation).

[3] Homogenization and group collapsing

In the core calculations with a huge amount of space-dependent data (cross section and neutron flux), the effective cross sections are processed, with a little degradation in accuracy as possible, by using the results from the multi-group lattice calculation. There are two processing methods. One is homogenization to lessen the space-dependent information and the other is group-collapsing to reduce the energy-dependent information as shown in Fig. 2.11. The fundamental idea of both methods is to conserve neutron reaction rate. In the homogenization, a homogenized neutron flux ϕ_g^{homo} is first defined as averaged flux weighted by volume V_k of region (k). Next, a homogenized cross section $\Sigma_{x,g}^{homo}$ is determined as satisfying Eq. (2.23) to represent the reaction rate in the homogenized whole region of volume V^{homo} . The fine-group neutron flux $\phi_{g,k}$ is used to calculate the homogenized cross section in Eq. (2.24).

$$\phi_g^{homo} \equiv \sum_k \phi_{g,k} V_k / \sum_k V_k = \sum_k \phi_{g,k} V_k / V^{homo} \quad (2.22)$$

$$\sum_{x,g}^{homo} \phi_g^{homo} V^{homo} = \sum_k \Sigma_{x,g,k} \phi_{g,k} V_k \quad (2.23)$$

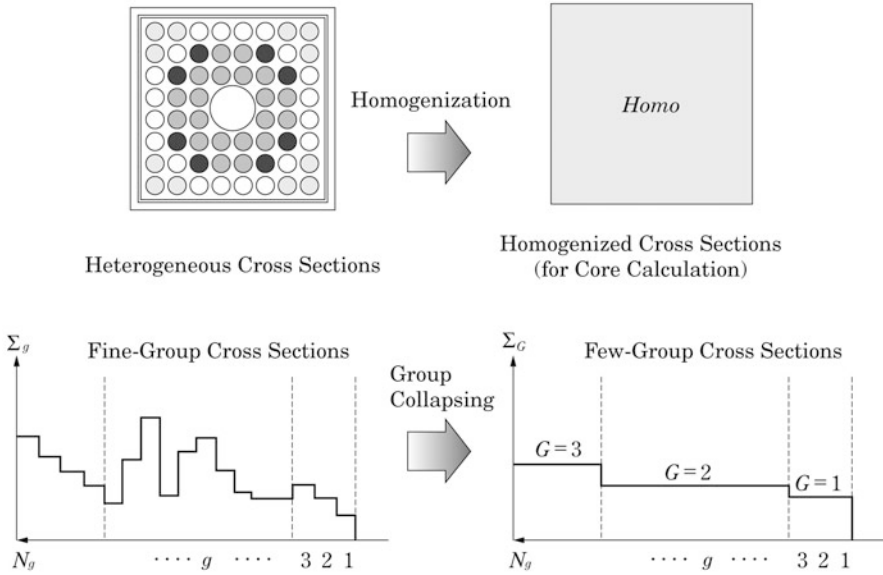


Fig. 2.11 Homogenization and group collapsing of cross section

$$\Sigma_{x,g}^{homo} \equiv \sum_k \Sigma_{x,g,k} \phi_{g,k} V_k / \phi_g^{homo} V^{homo} \equiv \sum_k \Sigma_{x,g,k} \phi_{g,k} V_k / \sum_k \phi_{g,k} V_k \quad (2.24)$$

Similarly, the homogenized microscopic cross section $\sigma_{x,g}^{i,homo}$ which represents the homogenized region is defined. First, the homogenized atomic number density $N^{i,homo}$ of nuclide i is defined from the following conservation of number of atoms

$$N^{i,homo} \equiv \sum_k N_k^i V_k / V^{homo} \quad (2.25)$$

The homogenized microscopic cross section is then given from the conservation of microscopic reaction rate of nuclide i as

$$\sigma_{x,g}^{i,homo} = \left(\sum_k N_k^i \sigma_{x,g,k}^i \phi_{g,k} V_k \right) / \left(N^{i,homo} \phi_g^{homo} V^{homo} \right) \quad (2.26)$$

Such homogenized neutron flux ϕ_g^{homo} and cross section $\Sigma_{x,g}^{homo}$ (or $\sigma_{x,g}^{i,homo}$) terms are used in performing the energy-group collapse. The fine-groups (g) are first apportioned to few-groups (G) for the core calculation as shown in Fig. 2.11. Since the multi-group neutron flux was obtained by the integration over its energy group, the few-group homogenized neutron flux can be represented by

$$\phi_G^{homo} \equiv \sum_{g \in G} \phi_g^{homo} \quad (2.27)$$

The next step is to consider the conservation of reaction rate in energy group G in the same manner as that in the homogenization.

The few-group homogenized macroscopic and microscopic cross sections are then given by

$$\Sigma_{x,G}^{homo} \equiv \sum_{g \in G} \Sigma_{x,g}^{homo} \phi_g^{homo} / \phi_G^{homo} = \sum_{g \in G} \Sigma_{x,g}^{homo} \phi_g^{homo} / \sum_{g \in G} \phi_g^{homo} \quad (2.28)$$

$$\sigma_{x,G}^{i,homo} \equiv \sum_{g \in G} \sigma_{x,g}^{i,homo} \phi_g^{homo} / \phi_G^{homo} = \sum_{g \in G} \sigma_{x,g}^{i,homo} \phi_g^{homo} / \sum_{g \in G} \phi_g^{homo} \quad (2.29)$$

The number of few-groups depends on reactor type and computation code. Two or three groups are adopted for the nuclear and thermal-hydraulic coupled core calculation of LWRs and about 18 groups are used for the core calculation of LMFRs. It should be noted that the conservation of reaction rate has been considered under the assumption that the lattice system can be represented as an infinite array of identical lattice cells. If the neutron spectrum in the actual core system is very different from the multi-group neutron spectrum calculated in the infinite lattice system, the applicability of such few-group homogenized cross sections to the core calculation is deteriorated. In this case, it is effective to increase the number of energy groups in the core calculation, but that gives a more costly computation.

[4] Lattice burnup calculation

The lattice burnup calculation prepares few-group homogenized cross sections with burnup on the infinite lattice system of fuel assembly. The series of lattice calculation procedures described in Fig. 2.8 are repeatedly done considering changes in fuel composition with burnup.

However, the lattice burnup calculation is not carried out in the design calculation of LMFRs which have a high homogeneity compared with LWRs and do not lead to a large change in neutron spectrum during burnup. Hence a macroscopic cross section at a position (\vec{r}) in the reactor core can be formed by Eq. (2.30) using the homogenized microscopic cross section prepared in the lattice calculation. At this time, the homogenized atomic number densities are calculated according to burnup of each region during the reactor core calculation.

$$\Sigma_{x,G}^{homo}(\vec{r}) = \sum_i N^{i,homo}(\vec{r}) \sigma_{x,G}^{i,homo} \quad (2.30)$$

By contrast, when considering ^{235}U in a fuel assembly of a LWR as an example, the constituents of UO_2 fuel, MOX fuel, or burnable poison fuel ($\text{UO}_2\text{-Gd}_2\text{O}_3$) each lead to different effective cross sections and composition variations with burnup. It is difficult to provide common few-group

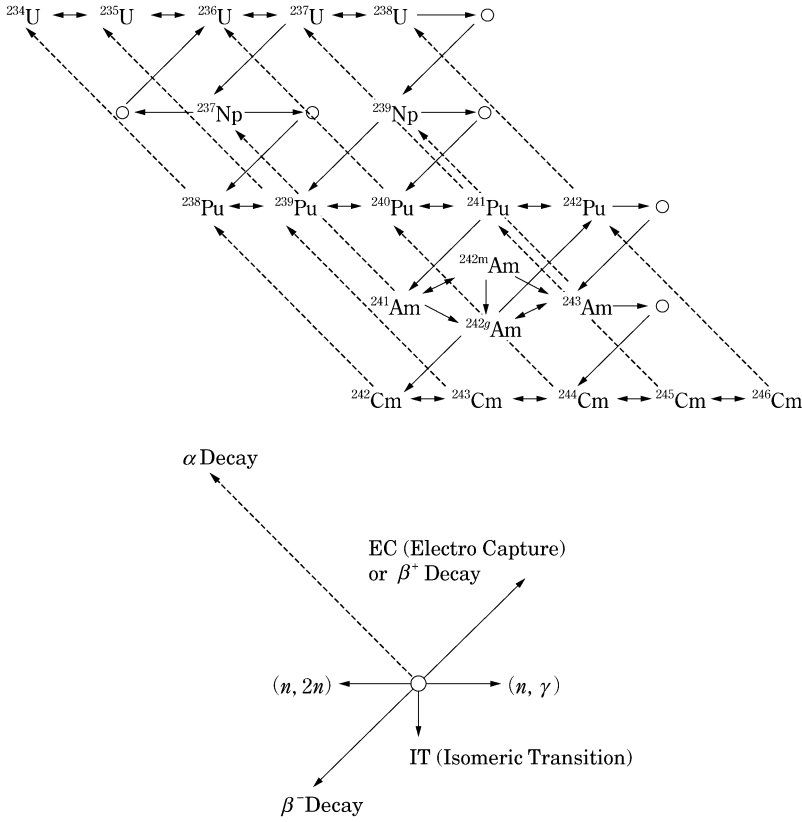


Fig. 2.12 An example burnup chain of heavy metals [7]

homogenized microscopic cross sections and homogenized atomic number densities suitable for all of them. Moreover, space-dependent lattice calculations by a fuel assembly model during the core calculation require an enormous computing time. In the design of reactors with this issue of fuel assembly homogenization, therefore, the lattice burnup calculation is performed in advance for the fuel assembly type of the core and then few-group homogenized macroscopic cross sections are tabulated with respect to burnup, etc. to be used for the core calculation. In the core calculation, macroscopic cross sections corresponding to burnup distribution in the core are prepared by interpolation of the table (the table interpolation method of macroscopic cross sections) [15].

Atomic number densities of heavy metals and fission products (FPs) are calculated along a burnup pathway as shown in Fig. 2.12, called the *burnup chain*.

The time variation in atomic number density (N^i) of a target nuclide (i) can be expressed as the following differential equation.

$$\frac{dN^i}{dt} = \sum_{j \neq i} f^{j \rightarrow i} \lambda^j N^j + \sum_{k \neq i} \sum_x g_x^{k \rightarrow i} N^k \langle \sigma_x^k \phi \rangle + \sum_l \gamma^{l \rightarrow i} F^l - (\lambda^i + \langle \sigma_a^i \phi \rangle) N^i \quad (2.31)$$

where the first term on the right-hand side expresses the production rate of nuclide i due to radioactive decay of another nuclide j on the burnup chain. λ^j is the decay constant of nuclide j and $f^{j \rightarrow i}$ is the probability (branching ratio) of decay to nuclide i . The second term is the production rate of nuclide i due to the nuclear reaction x of another nuclide k . The major nuclear reaction is the neutron capture reaction and other reactions such as the $(n,2n)$ reaction can be considered by necessity. $\langle \sigma_x^k \phi \rangle$, which is the microscopic reaction rate of nuclide k integrated over all neutron energies, is calculated from the fine-group effective cross section and neutron flux in the lattice calculation. $g_x^{k \rightarrow i}$ is the probability of transmutation into nuclide i for nuclear reaction x of nuclide k . The third term is for the production of FPs. F^l is the fission rate of heavy nuclide l and $\gamma^{l \rightarrow i}$ is the production probability (yield fraction) of nuclide i for the fission reaction. The last term is the loss rate of nuclide i due to radioactive decay and absorption reactions.

Applying Eq. (2.31) to all nuclides including FPs on the burnup chain gives simultaneous differential equations (burnup equations) corresponding to the number of nuclides. Ways to solve the burnup equations include the Bateman method [16] and the matrix exponential method [17]. This burnup calculation, called the *depletion calculation*, is performed for each burnup region in case of multiple burnup regions like a fuel assembly and it gives the variation in material composition with burnup in each region. The lattice calculation is carried out with the material composition repeatedly until reaching maximum burnup expected in the core.

The infinite multiplication factor calculated during the lattice calculation is described as the ratio between neutron production and absorption reactions in an infinite lattice system without neutron leakage.

$$\begin{aligned} k_\infty &= \text{Production Rate} / \text{Loss Rate} \\ &= \text{Production Rate} / (\text{Absorption Rate} + \text{Leakage Rate from System}) \\ &= \text{Production Rate} / (\text{Absorption Rate} + 0.0) \\ &= \sum_{g \in G} v \Sigma_{f,g}^{homo} \phi_g^{homo} / \sum_{g \in G} \Sigma_{a,g}^{homo} \phi_g^{homo} \end{aligned} \quad (2.32)$$

Figure 2.13 shows the infinite multiplication factor obtained from the lattice burnup calculation of a BWR fuel assembly. Since thermal reactors rapidly produce highly neutron absorbing FPs such as ^{135}Xe and ^{149}Sm in the beginning of burnup until their concentrations reach the equilibrium values, the infinite

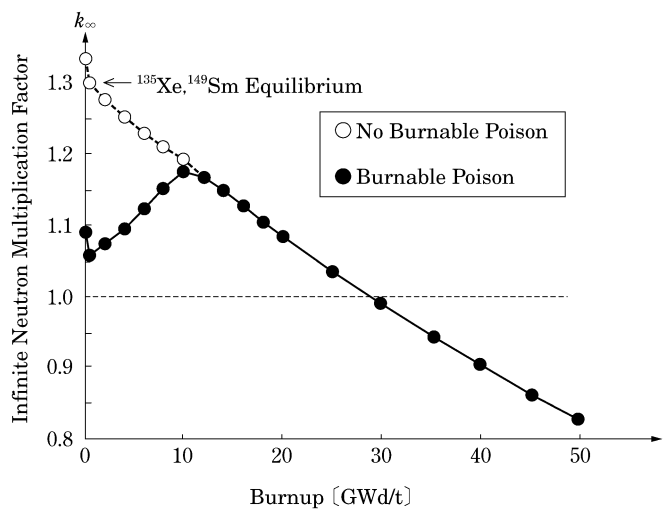


Fig. 2.13 Lattice burnup calculation of fuel assembly

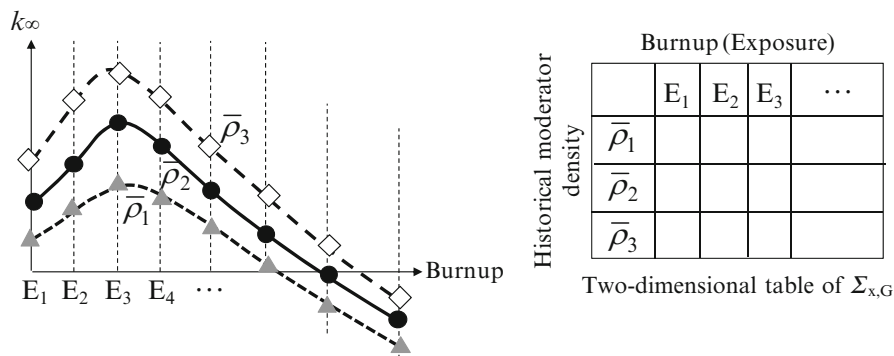
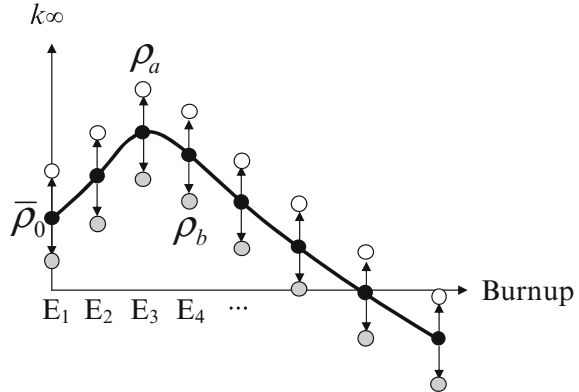


Fig. 2.14 Tabulation of few-group homogenized macroscopic cross sections in lattice burnup calculations

multiplication factor sharply drops during a short time. Then the infinite multiplication factor monotonously decreases in the case of no burnable poison fuel ($\text{UO}_2 + \text{Gd}_2\text{O}_3$). Meanwhile, it increases once in burnable poison fuel because burnable poisons burn out gradually with burnup, and then it decreases when the burnable poisons become ineffective.

The few-group homogenized macroscopic cross sections are tabulated at representative burnup steps (E_1, E_2, E_3, \dots) by the lattice burnup calculation and stored as a reactor constant library for the core calculation, as shown in Fig. 2.14. Three different moderator densities ($\bar{\rho}_1, \bar{\rho}_2, \bar{\rho}_3$) for one fuel type are assumed in the lattice burnup calculation of BWRs. Moderator density of BWRs

Fig. 2.15 Branch-off calculation of moderator density



is provided as a function of void fraction α for two densities ρ_l and ρ_g in liquid and vapor phases, respectively, in the steam table. That is, it is given by

$$\bar{\rho} = \rho_l(1 - \alpha) + \rho_g\alpha \quad (2.33)$$

where $\bar{\rho}_1$, $\bar{\rho}_2$, and $\bar{\rho}_3$ are the moderator densities corresponding to each void fraction at the core outlet ($\alpha = 0.7$), as an average ($\alpha = 0.4$), and at the inlet ($\alpha = 0.0$) of typical BWRs. Since this moderator density is assumed to be constant as an average value during each lattice burnup step, it is called a *historical moderator density*.

The few-group homogenized macroscopic cross sections are tabulated according to two historical parameters (burnup E and historical moderator density $\bar{\rho}$) by energy group (G) or cross section type (x). The cross section tables are prepared individually according to fuel type (F), control rod insertion or withdrawal, etc. Furthermore, homogenized microscopic cross sections and atomic number densities of ^{135}Xe , ^{149}Sm , ^{10}B , etc. can be tabulated by necessity.

[5] Branch-off calculation

In the lattice burnup calculation, a combination of parameters such as moderator density and temperature, and fuel temperature is made at representative values $(\bar{\rho}_0, T_{m0}, T_{f0})$ expected at normal operation of the reactor. In the core calculation, however, a different set (ρ, T_m, T_f) from the representative set is taken depending on position and time. Hence, a subsequent calculation called the *branch-off calculation* is performed after the lattice burnup calculation if necessary.

Figure 2.15 depicts an example branch-off calculation of moderator density. The calculation proceeds in the following order:

- (i) Perform the lattice burnup calculation at a reference condition $(\bar{\rho}_0, T_{m0}, T_{f0})$. Designate the few-group homogenized cross section prepared from the lattice burnup calculation as $\Sigma(\bar{\rho}_0, T_{m0}, T_{f0})$.

- (ii) Perform the lattice calculation at each burnup step on the condition that only the moderator density is changed from $\bar{\rho}_0$ to ρ_a , by using the same fuel composition at each burnup step. Designate the few-group homogenized cross section prepared from the lattice calculation (or the branch-off calculation) as $\Sigma(\bar{\rho}_0 \rightarrow \rho_a, T_{m0}, T_{f0})$.
- (iii) Carry out the branch-off calculation similar to (ii) at another moderator density of ρ_b and give $\Sigma(\bar{\rho}_0 \rightarrow \rho_b, T_{m0}, T_{f0})$.
- (iv) If the moderator density is instantaneously changed from $\bar{\rho}_0$ to an arbitrary ρ , calculate the corresponding cross section by the following approximation (quadratic fitting).

$$\Sigma(\bar{\rho}_0 \rightarrow \rho, T_{m0}, T_{f0}) \approx \Sigma(\bar{\rho}_0, T_{m0}, T_{f0}) + a(\rho - \bar{\rho}_0) + b(\rho - \bar{\rho}_0)^2 \quad (2.34)$$

- (v) Determine the fitting coefficients a and b from the approximation at $\rho = \rho_a$ and $\rho = \rho_b$.

Hence, the cross section at an arbitrary moderator density (an instantaneous moderator density) ρ away from the historical moderator density $\bar{\rho}_0$ can be expressed by the method mentioned above. If three moderator densities ($\bar{\rho}_1, \bar{\rho}_2, \bar{\rho}_3$) are employed as $\bar{\rho}_0$ as shown in Fig. 2.14, their branch-off calculations can give $\Sigma(\bar{\rho}_1 \rightarrow \rho, T_{m0}, T_{f0})$, $\Sigma(\bar{\rho}_2 \rightarrow \rho, T_{m0}, T_{f0})$, and $\Sigma(\bar{\rho}_3 \rightarrow \rho, T_{m0}, T_{f0})$. By interpolation of the three points, the cross section at ρ resulting from an instantaneous change from a historical moderator density $\bar{\rho}$ can be obtained as $\Sigma(\bar{\rho} \rightarrow \rho, T_{m0}, T_{f0})$.

The cross section at an instantaneous change in fuel or moderator temperature can also be described by the same function fitting as above. Since its change in cross section is not as large as a void fraction change (0–70 %), the following linear fittings are often used.

$$\Sigma(\bar{\rho}_0, T_{m0} \rightarrow T_{m0}, T_{f0}) = \Sigma(\bar{\rho}_0, T_{m0}, T_{f0}) + c(T_m - T_{m0}) \quad (2.35)$$

$$\Sigma(\bar{\rho}_0, T_{m0}, T_{f0} \rightarrow T_f) = \Sigma(\bar{\rho}_0, T_{m0}, T_{f0}) + d(\sqrt{T_f} - \sqrt{T_{f0}}) \quad (2.36)$$

Equation (2.36) has square roots of fuel temperature in order to express the cross section change due to the Doppler effect by a lower-order fitting equation. An employment of a higher-order fitting equation can lead to a higher expression capability and accuracy, but it gives rise to a substantial increase in the number of branch-off calculations and fitting coefficients and therefore results in an inefficient calculation. Thus, the reference cross sections and their fitting coefficients are stored into the few-group reactor constant library and used in the nuclear and thermal-hydraulic coupled core calculation.

2.1.5 Core Calculation

[1] Diffusion equation

In core calculations such as the nuclear and thermal-hydraulic coupled core calculation, core burnup calculation, or space-dependent kinetics calculation, high-speed calculation is the biggest need. Especially since large commercial reactors have a considerably larger core size compared with critical assemblies or experimental reactors, the neutron transport equation (2.1) has to take many unknowns and hence need a high computing cost.

For most core calculations, the angular dependence ($\vec{\Omega}$) of neutron flux is disregarded and the neutron transport equation is approximately simplified as Eq. (2.37).

$$\frac{1}{v} \frac{\partial \phi}{\partial t} = -\nabla \cdot \vec{J} - \Sigma_a \phi + S \quad (2.37)$$

Its physical meaning is simple. As an example, a space of unit volume (1 cm^3) like one die of a pair of dice is considered. The time variation in neutron population within the space [the LHS of Eq. (2.37)] is then given by the balanced relationship between neutron production rate (S), net neutron leakage rate through the surface ($\nabla \cdot \vec{J}$), and neutron loss rate by absorption ($\Sigma_a \phi$).

\vec{J} is referred to as the *net neutron current* and expressed by the following physical relation known as Fick's law

$$\vec{J} = -D \nabla \phi \quad (2.38)$$

where D is called the *diffusion coefficient*; it is tabulated together with few-group cross sections in the lattice calculation to be delivered to the core calculation. Inserting Eq. (2.38) into Eq. (2.37) gives the time-dependent diffusion equation.

$$\frac{1}{v} \frac{\partial \phi}{\partial t} = \nabla \cdot D \nabla \phi - \Sigma_a \phi + S \quad (2.39)$$

The time-independent form of Eq. (2.39) is the steady-state diffusion equation and all types of the core calculation to be mentioned thereafter are based on the equation

$$\nabla \cdot D \nabla \phi - \Sigma_a \phi + S = 0 \quad (2.40)$$

Thus, solving the diffusion equation in critical reactors is to regard the reactor core as an integration of subspaces like the dice cubes and then to find a neutron flux distribution to satisfy the neutron balance between production and loss in all the spaces (corresponding to mesh spaces to be described later).

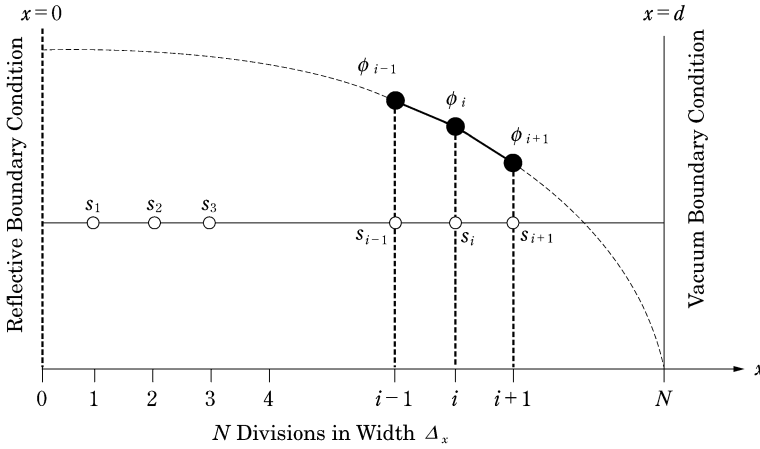


Fig. 2.16 Finite difference in 1D plane geometry

[2] Solution to one-dimensional (1D) one-group diffusion equation by finite difference method

First a non-multiplying medium (e.g., water) is considered for simplicity of the equation, though practical systems are composed of various materials with different cross sections. In addition, it is assumed that all neutrons can be characterized by a single energy (one-group problem). Therefore, the cross section does not depend on location and in this case the diffusion equation is given by Eq. (2.41).

$$DV^2\phi - \Sigma_a\phi + S = 0 \quad (2.41)$$

∇^2 (the Laplacian operator) is dependent on the coordinate system and in the Cartesian coordinate system it is represented as Eq. (2.42).

$$\nabla^2 = \frac{\partial^2}{\partial x^2} + \frac{\partial^2}{\partial y^2} + \frac{\partial^2}{\partial z^2} \quad (2.42)$$

In an infinitely wide medium in y and z directions, the diffusion equation reduces to the 1D form.

$$-D \frac{d^2\phi(x)}{dx^2} + \Sigma_a\phi(x) = S(x) \quad (2.43)$$

Here a uniform neutron source ($s_1 = s_2 = s_3 \dots = s$) in a finite slab of width $2d$ is considered as shown in Fig. 2.16 and the finite difference method to solve for neutron flux distribution is discussed. The reflective boundary condition is applied to the center of the slab and one side of width d is divided into equal N regions (spatial meshes). The second-order derivative of Eq. (2.43) can be

approximated¹ by using neutron flux ϕ_i at a mesh boundary i and neutron fluxes at both adjacent sides as follows;

$$\left. \frac{d^2\phi}{dx^2} \right|_i \approx \frac{\left\{ \left(\frac{\phi_{i+1} - \phi_i}{\Delta_x} \right) - \left(\frac{\phi_i - \phi_{i-1}}{\Delta_x} \right) \right\}}{\Delta_x} = \frac{\phi_{i-1} - 2\phi_i + \phi_{i+1}}{\Delta_x^2} \quad (2.44)$$

Hence the diffusion equation at each mesh point can be given by

$$-D \left(\frac{\phi_{i-1} - 2\phi_i + \phi_{i+1}}{\Delta_x^2} \right) + \Sigma_a \phi_i = s_i \quad (i=1 \sim N-1) \quad (2.45)$$

It can be rewritten by

$$\left(\frac{1}{\Delta_x^2} \right) \phi_{i-1} + \left(\frac{-2}{\Delta_x^2} + \frac{-1}{D/\Sigma_a} \right) \phi_i + \left(\frac{1}{\Delta_x^2} \right) \phi_{i+1} = \left(-\frac{s_i}{D} \right) \quad (i=1 \sim N-1) \quad (2.46)$$

where

$$a \equiv \left(\frac{1}{\Delta_x^2} \right), \quad b \equiv \left(\frac{-2}{\Delta_x^2} + \frac{-1}{D/\Sigma_a} \right), \quad S_i \equiv \left(-\frac{s_i}{D} \right) \quad (2.47)$$

In the case of $N = 5$, the following simultaneous equations are gotten.

$$\begin{cases} a\phi_0 + b\phi_1 + a\phi_2 = S_1 \\ a\phi_1 + b\phi_2 + a\phi_3 = S_2 \\ a\phi_2 + b\phi_3 + a\phi_4 = S_3 \\ a\phi_3 + b\phi_4 + a\phi_5 = S_4 \end{cases} \quad (2.48)$$

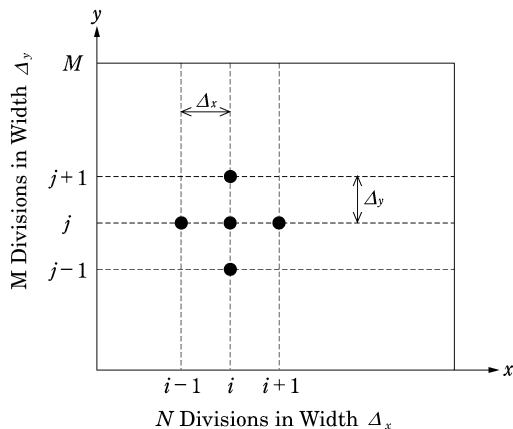
Since there are six unknowns (ϕ_0 to ϕ_5) among four equations in Eq. (2.48), another two conditions are needed to solve the simultaneous equations. Boundary conditions at both ends ($x = 0$ and $x = d$) of the slab are given by the following.

Vacuum boundary condition (an extrapolated distance is assumed zero):

$$\phi(x = d) = 0 \quad \rightarrow \quad \phi_5 = 0 \quad (2.49)$$

¹Most practical codes of the finite difference method take neutron fluxes at the center points of divided meshes [13]. A simple and easy to understand method was employed here.

Fig. 2.17 Finite difference in 2D plane geometry



Reflective boundary condition:

$$\left. \frac{d\phi}{dx} \right|_{x=0} = 0 \rightarrow \frac{\phi_1 - \phi_0}{\Delta x} = 0 \quad (2.50)$$

Equation (2.51) is obtained by inserting Eqs. (2.49) and (2.50) into Eq. (2.48) and rewriting in matrix form.

$$\begin{bmatrix} a+b & a & 0 & 0 \\ a & b & a & 0 \\ 0 & a & b & a \\ 0 & 0 & a & b \end{bmatrix} \begin{bmatrix} \phi_1 \\ \phi_2 \\ \phi_3 \\ \phi_4 \end{bmatrix} = \begin{bmatrix} S_1 \\ S_2 \\ S_3 \\ S_4 \end{bmatrix} \quad (2.51)$$

A 1D problem generally results in a tridiagonal matrix equation of $(N - 1) \times (N - 1)$ system which can be directly solved using numerical methods such as the Gaussian elimination method. Since the finite difference method introduces the approximation as Eq. (2.44), it is necessary to choose a sufficiently small mesh spacing. The spatial variation of neutron flux is essentially characterized by the extent of neutron diffusion such as the neutron mean free path. Hence the effect of the mesh size on nuclear characteristic evaluations of a target reactor core must be understood and then the mesh size is optimized relative to the computation cost.

[3] Solution of the multi-dimensional diffusion equation

The diffusion equation in a 2D homogeneous plane geometry is given by Eq. (2.52).

$$-D \left(\frac{\partial^2 \phi(x, y)}{\partial x^2} + \frac{\partial^2 \phi(x, y)}{\partial y^2} \right) + \Sigma_a \phi(x, y) = S(x, y) \quad (2.52)$$

The plane is divided into N and M meshes in x and y directions, respectively (Fig. 2.17). Similarly to the 1D problem, the second-order derivatives can be

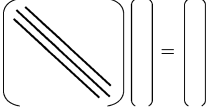
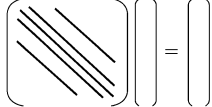
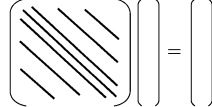
1D Problem	2D Problem	3D Problem
		
3-Point Difference Equations	5-Point Difference Equations	7-Point Difference Equations
Tridiagonal Matrix of (N-1) × (N-1)	5-Diagonal Matrix of {(N-1)(M-1)} ²	7-Diagonal Matrix of {(N-1)(M-1)(K-1)} ²

Fig. 2.18 Matrix equation forms of finite difference method

approximated by using neutron fluxes at a point (i, j) and its four adjacent ones as the following.

$$\left. \frac{\partial^2 \phi}{\partial x^2} \right|_{i,j} \approx \frac{\phi_{i-1,j} - 2\phi_{i,j} + \phi_{i+1,j}}{\Delta_x^2} \quad (2.53)$$

$$\left. \frac{\partial^2 \phi}{\partial y^2} \right|_{i,j} \approx \frac{\phi_{i,j-1} - 2\phi_{i,j} + \phi_{i,j+1}}{\Delta_y^2} \quad (2.54)$$

Hence the diffusion equation at each mesh point can be given by

$$-D \left(\frac{\phi_{i-1,j} - 2\phi_{i,j} + \phi_{i+1,j}}{\Delta_x^2} + \frac{\phi_{i,j-1} - 2\phi_{i,j} + \phi_{i,j+1}}{\Delta_y^2} \right) + \Sigma_a \phi_{i,j} = s_{i,j} \quad (2.55)$$

$(i = 1 \text{ to } N-1, j = 1 \text{ to } M-1)$

and it can be rewritten as Eq. (2.56).

$$\begin{aligned} & \left(\frac{1}{\Delta_x^2} \right) \phi_{i-1,j} + \left(\frac{1}{\Delta_y^2} \right) \phi_{i,j-1} + \left(\frac{-2}{\Delta_x^2} + \frac{-2}{\Delta_y^2} + \frac{-1}{D/\Sigma_a} \right) \phi_{i,j} + \left(\frac{1}{\Delta_x^2} \right) \phi_{i+1,j} + \left(\frac{1}{\Delta_y^2} \right) \phi_{i,j+1} \\ & = \left(-\frac{s_{i,j}}{D} \right) \quad (i = 1 \text{ to } N-1, j = 1 \text{ to } M-1) \end{aligned} \quad (2.56)$$

Next, the corresponding simultaneous equations are expressed in matrix form, similarly to the 1D problem except four boundary conditions are used: two conditions in each of the x and y directions.

A 3D problem even in a different coordinate system basically follows the same procedure and a matrix form of $[A]\phi = S$ can be taken as shown in Fig. 2.18.

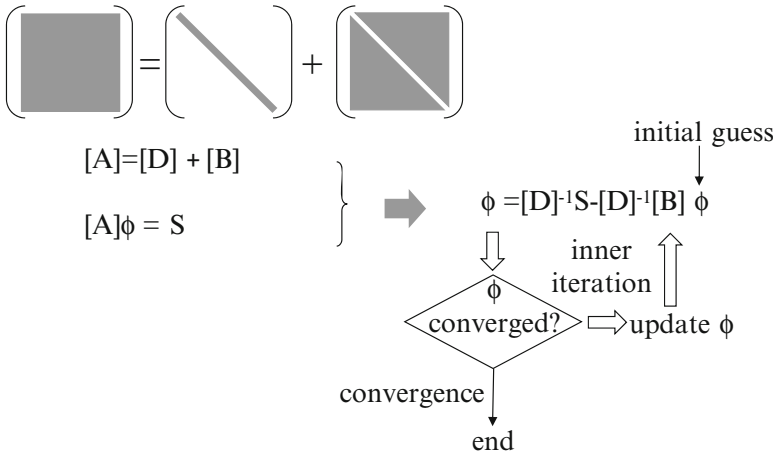


Fig. 2.19 Inner iteration to solve a system of equations

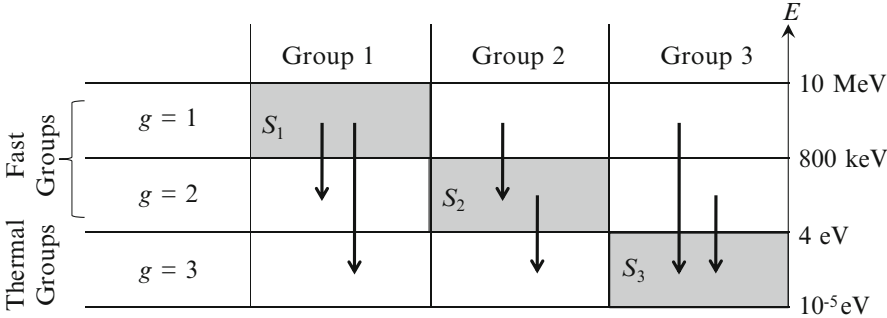


Fig. 2.20 Slowing-down neutron balance in three-group problem

In the case of a large-size matrix $[A]$, a direct method such as the Gaussian elimination leads to increased necessary memory size and it is liable to cause accumulation of numerical errors as well. Hence, generally first the matrix $[A]$ is composed into its diagonal element $[D]$ and off-diagonal element $[B]$. Then ϕ is guessed and new guesses are calculated iteratively to converge to the true solution (Fig. 2.19). This iterative algorithm, such as found in the Gauss-Seidel method or the successive overrelaxation (SOR) method, is frequently referred to as the *inner iteration*.

[4] Solution to multi-group diffusion equation

As already mentioned, the diffusion equation is a balanced equation between neutron production and loss. The multi-group diffusion theory is similarly considered except that the neutron energy is discretized into multi-groups. As shown in Fig. 2.20, subsequent treatment should be made for neutrons moving

to other groups through slowing down which is not considered in the one-group diffusion theory. In particular, there are two points:

- (i) Neutrons which move out of a target group to other groups by slowing down result in neutron loss in the neutron balance of the target group.
- (ii) Neutrons which move in a target group from other groups by slowing down result in neutron gain in the neutron balance of the target group.

Hence, the multi-group diffusion equation introduces the cross section $\Sigma_{g \rightarrow g'}$ (scattering matrix) characterizing neutrons which transfer from group g to group g' by elastic or inelastic scattering.

In the example of the three-group problem presented in Fig. 2.20, the neutron balance equation of each group can be given by

$$\text{Group 1: } D_1 \nabla^2 \phi_1 - (\Sigma_{a,1} \phi_1 + \Sigma_{1 \rightarrow 2} \phi_1 + \Sigma_{1 \rightarrow 3} \phi_1) + S_1 = 0 \quad (2.57)$$

$$\text{Group 2: } D_2 \nabla^2 \phi_2 - (\Sigma_{a,2} \phi_2 + \Sigma_{2 \rightarrow 3} \phi_2) + (S_2 + \Sigma_{1 \rightarrow 2} \phi_1) = 0 \quad (2.58)$$

$$\text{Group 3: } D_3 \nabla^2 \phi_3 - (\Sigma_{a,3} \phi_3) + (S_3 + \Sigma_{1 \rightarrow 3} \phi_1 + \Sigma_{2 \rightarrow 3} \phi_2) = 0 \quad (2.59)$$

It is seen that neutron loss due to slowing down in a group results in neutron gains in other groups. $\Sigma_{1 \rightarrow 2} \phi_1$ in Eq. (2.58) and $\Sigma_{1 \rightarrow 3} \phi_1 + \Sigma_{2 \rightarrow 3} \phi_2$ in Eq. (2.59) are referred to as the “slowing-down neutron source” since they represent the neutron source due to slowing down from other groups.

Equation (2.57) for group 1 can be rewritten as the following.

$$\nabla^2 \phi_1 - \Sigma_{r,1} \phi_1 + S_1 = 0 \quad (2.60)$$

$$\Sigma_{r,1} \equiv \Sigma_{a,1} + \Sigma_{1 \rightarrow 2} + \Sigma_{1 \rightarrow 3} \quad (2.61)$$

The sum of absorption cross section and group-transfer cross section, namely, the cross section which characterizes neutrons removed from the target group, is called the *removal cross section*. It is observed that Eq. (2.60) rewritten using the removal cross section is in the same form as the one-group diffusion equation and can be solved by the finite difference method mentioned before. Substituting the obtained ϕ_1 for the one in the slowing-down source of Eq. (2.58) makes it possible to calculate the neutron flux of group 2, ϕ_2 , in the same way. Further, the neutron flux of group 3, ϕ_3 , can be also obtained by substituting ϕ_1 and ϕ_2 into Eq. (2.59).

Thus, the multi-group diffusion equations can be solved in sequence from the highest energy group. However, the solution is not obtained by this method if the thermal energy region (up to about 4 eV) is divided into multi-groups. As an example, a four-group diffusion problem using two fast groups and two thermal groups is considered.

$$\text{Group 1: } D_1 \nabla^2 \phi_1 - (\Sigma_{a,1} \phi_1 + \Sigma_{1 \rightarrow 2} \phi_1 + \Sigma_{1 \rightarrow 3} \phi_1 + \Sigma_{1 \rightarrow 4} \phi_1) + S_1 = 0 \quad (2.62)$$

$$\text{Group 2: } D_2 \nabla^2 \phi_2 - (\Sigma_{a,2} \phi_2 + \Sigma_{2 \rightarrow 3} \phi_2 + \Sigma_{2 \rightarrow 4} \phi_2) + (S_2 + \Sigma_{1 \rightarrow 2} \phi_1) = 0 \quad (2.63)$$

$$\begin{aligned} \text{Group 3: } D_3 \nabla^2 \phi_3 - (\Sigma_{a,3} \phi_3 + \Sigma_{3 \rightarrow 4} \phi_3) + (S_3 + \Sigma_{1 \rightarrow 3} \phi_1 + \Sigma_{2 \rightarrow 3} \phi_2 + \Sigma_{4 \rightarrow 3} \phi_4) \\ = 0 \end{aligned} \quad (2.64)$$

$$\text{Group 4: } D_4 \nabla^2 \phi_4 - (\Sigma_{a,4} \phi_4) + (S_4 + \Sigma_{1 \rightarrow 4} \phi_1 + \Sigma_{2 \rightarrow 4} \phi_2 + \Sigma_{3 \rightarrow 4} \phi_3) = 0 \quad (2.65)$$

The fast-group neutron fluxes ϕ_1 and ϕ_2 can be derived by the same procedure as in the previous three-group problem. In the thermal groups, however, an event that a neutron gains kinetic energy in a collision with a moderator nuclide in thermal vibration, that is, the upscattering of thermal neutrons should be considered. The last term of Eq. (2.64) represents that. Thus, since the neutron source terms for group 3 include the unknown neutron flux of group 4, ϕ_4 , it is impossible to directly solve the equation. Here, a guess $\phi_4^{(0)}$ instead of ϕ_4 is taken at Eq. (2.64) and then a solution $\phi_3^{(1)}$ is given. Moreover, a solution $\phi_4^{(1)}$ is also acquired by the substitution of $\phi_3^{(1)}$ into Eq. (2.65). Since $\phi_3^{(1)}$ and $\phi_4^{(1)}$ are not correct solutions, another new guess $\phi_4^{(1)}$ is used in Eq. (2.64) to obtain $\phi_3^{(2)}$, which is substituted again into Eq. (2.65) to acquire $\phi_4^{(2)}$. Such calculations are iteratively performed until $\phi_3^{(n)}$ and $\phi_4^{(n)}$ come to an agreement with each previous $\phi_3^{(n-1)}$ and $\phi_4^{(n-1)}$. This calculation is referred to as the “thermal iteration” calculation.

The codes developed for core design of only fast reactors may have no such upscattering and iteration calculation function or may cut back the slowing-down groups by assuming collisions with only heavy metal elements such as sodium. Since such codes cannot correctly manage transport calculation of thermal neutrons, they should not be used carelessly in a thermal reactor calculation even though the codes solve the same fundamental equation.

[5] Eigenvalue problem with fission source

So far the diffusion equation has been discussed in a non-multiplying medium with an external neutron source. Here, fission neutron production (fission source) in a reactor core is applied to the diffusion equation. Assuming a volumetric fission reaction rate $\Sigma_f \phi$ and an average number of neutrons released per fission ν in a unit cubic volume (1 cm^3) leads to a volumetric fission neutron production rate by multiplying both ones. Hence, substituting the fission source $\nu \Sigma_f \phi$ for the external source (S) in Eq. (2.41) gives the one-group diffusion equation at the steady-state reactor core as the following.

$$D\nabla^2\phi - \Sigma_a\phi + \nu\Sigma_f\phi = 0 \quad (2.66)$$

This equation represents a complete balance between the number of neutrons produced by fission and the number of neutrons lost due to leakage and absorption, in an arbitrary unit volume at the critical condition of the reactor. In actual practice, however, it is hard to completely meet such a balance in the design calculation step. A minor transformation of Eq. (2.66) can be made as

$$-D\nabla^2\phi + \Sigma_a\phi = \frac{\nu\Sigma_f}{k_{eff}}\phi \quad (2.67)$$

where k_{eff} is an inherent constant characterizing the system, called the *eigenvalue*. If $k_{eff} = 1.0$, Eq. (2.67) becomes identical to Eq. (2.66). The equation may be solved for the eigenvalue k_{eff} :

$$k_{eff} = \frac{(\nu\Sigma_f\phi)}{(-D\nabla^2\phi) + (\Sigma_a\phi)} = \frac{P}{L + A} \quad (2.68)$$

where L , A , and P denote neutron leakage, absorption, and production, respectively. If the space is extended to the whole reactor core (i.e., each term is integrated over the whole reactor core), k_{eff} can be interpreted as follows. The numerator is the number of neutrons that will be born in the reactor core in the next generation, whereas the denominator represents those that are lost from the current generation. Hence, the condition of the reactor core depends on the k_{eff} value as given next.

$$\begin{cases} k_{eff} > 1 : \text{Supercritical} \\ k_{eff} = 1 : \text{Critical} \\ k_{eff} < 1 : \text{Subcritical} \end{cases} \quad (2.69)$$

Another interpretation can be given for k_{eff} in Eq. (2.67). As mentioned above, it is highly unlikely to hit on the exact neutron balance of $L + A = P$ in a practical core design calculation. Neither the supercritical ($L + A < P$) nor subcritical ($L + A > P$) condition gives a steady-state solution to Eq. (2.66). Hence, if k_{eff} is introduced into the equation as an adjustment parameter like Eq. (2.67), the neutron balance can be forced to maintain ($P \rightarrow P/k_{eff}$) and the equation will always have a steady-state solution. In a supercritical condition ($k_{eff} > 1$), for example, the neutron balance can be kept by adjusting down the neutron production term ($\nu\Sigma_f\phi \rightarrow \nu\Sigma_f\phi/k_{eff}$).

A problem expressed as an equation in the form of Eq. (2.67) is referred to as an *eigenvalue problem*. By contrast, a problem with an external neutron source such as Eq. (2.41) is referred to as a *fixed-source problem*. The big difference between both equations is that the eigenvalue problem equation has an infinite set of solutions. For example, if ϕ is a solution of Eq. (2.67), it is self-evident

that 2ϕ and 3ϕ are also other solutions. Consequently, the solutions of the eigenvalue problem are not absolute values of ϕ but the eigenvalue k_{eff} and a relative spatial distribution of ϕ . Meanwhile, the fixed-source problem has a spatial distribution of absolute ϕ which is proportional to the intensity of the external neutron source.

[6] Solution to multi-group eigenvalue problem

The diffusion equation of the eigenvalue problem by the one-group theory [Eq. (2.67)] can be extended to an equation based on the multi-group theory and its numerical solutions are discussed here.

In the eigenvalue problem of the multi-group theory, it is necessary to describe the fission source term ($\nu\Sigma_f\phi$) in the multi-group form as well as the loss and production terms due to the neutron slowing-down. Since the fission reaction occurs in all energy groups, the total production rate of fission neutrons in the unit volume is given by Eq. (2.70).

$$P = \nu\Sigma_{f,1}\phi_1 + \nu\Sigma_{f,2}\phi_2 + \nu\Sigma_{f,3}\phi_3 \cdots = \sum_{g'} \nu\Sigma_{f,g'}\phi_{g'} \quad (2.70)$$

The probability that a fission neutron will be born with an energy in group g is given by

$$\chi_g = \int_{\Delta E_g} \chi(E) dE \quad (2.71)$$

where $\chi(E)$ is the fission neutron spectrum normalized to unity and therefore the sum of χ_g is the same unity.

$$\sum_g \chi_g = 1.0 \quad (2.72)$$

Hence, the fission source of group g can be expressed as Eq. (2.73).

$$\chi_g P = \chi_g \sum_{g'} \nu\Sigma_{f,g'}\phi_{g'} \quad (2.73)$$

For the three-group problem (fixed-source problem) of Fig. 2.20, replacement of the external source by the fission source is considered. If S_g is substituted by $\chi_g P/k_{eff}$ in Eqs. (2.57), (2.58), and (2.59), then the following diffusion equations are given for three-group eigenvalue problem:

$$\text{Group 1: } -D_1 \nabla^2 \phi_1 + (\Sigma_{a,1}\phi_1 + \Sigma_{1 \rightarrow 2}\phi_1 + \Sigma_{1 \rightarrow 3}\phi_1) = \frac{\chi_1 P}{k_{eff}} \quad (2.74)$$

$$\text{Group 2: } -D_2 \nabla^2 \phi_2 + (\Sigma_{a,2}\phi_2 + \Sigma_{2 \rightarrow 3}\phi_2) = \frac{\chi_2 P}{k_{eff}} + \Sigma_{1 \rightarrow 2}\phi_1 \quad (2.75)$$

$$\text{Group 3: } -D_3 \nabla^2 \phi_3 + (\Sigma_{a,3} \phi_3) = \frac{\chi_3 P}{k_{eff}} + (\Sigma_{1 \rightarrow 3} \phi_1 + \Sigma_{2 \rightarrow 3} \phi_2) \quad (2.76)$$

where

$$P = \nu \Sigma_{f,1} \phi_1 + \nu \Sigma_{f,2} \phi_2 + \nu \Sigma_{f,3} \phi_3 \quad (2.77)$$

In the three-group fixed-source problem, it was seen that the diffusion equations are solved in consecutive order from group 1. However, Eqs. (2.74), (2.75), and (2.76) have the fission source P which includes ϕ_1 , ϕ_2 , and ϕ_3 , and moreover k_{eff} is unknown. Hence, iterative calculations are performed as the next sequence.

- (i) Guess $k_{eff}^{(0)}$ for k_{eff} , and $\phi_1^{(0)}$, $\phi_2^{(0)}$, and $\phi_3^{(0)}$ for determining P . It is common to begin with an initial guess of $k_{eff}^{(0)} = 1.0$ and a flat distribution of the neutron fluxes (constant values).
- (ii) Since neutron fluxes are relative and arbitrary values in eigenvalue problems, normalize the initial neutron fluxes to satisfy Eq. (2.78).

$$k_{eff}^{(0)} = \int_{core} \nu \Sigma_{f,1} \phi_1^{(0)} + \nu \Sigma_{f,2} \phi_2^{(0)} + \nu \Sigma_{f,3} \phi_3^{(0)} dV \quad (2.78)$$

Since fission source terms are divided by k_{eff} in eigenvalue diffusion equations, Eq. (2.78) indicates that the total neutron source in the system is normalized to a value of 1 to fit into the next diffusion equation.

- (iii) Provide $P^{(0)}$ of Eq. (2.79) with the RHS of Eq. (2.80) and then solve this for $\phi_1^{(1)}$.

$$P^{(0)} = \nu \Sigma_{f,1} \phi_1^{(0)} + \nu \Sigma_{f,2} \phi_2^{(0)} + \nu \Sigma_{f,3} \phi_3^{(0)} \quad (2.79)$$

$$\text{Group 1: } -D_1 \nabla^2 \phi_1^{(1)} + (\Sigma_{a,1} + \Sigma_{1 \rightarrow 2} + \Sigma_{1 \rightarrow 3}) \phi_1^{(1)} = \frac{\chi_1 P^{(0)}}{k_{eff}^{(0)}} \quad (2.80)$$

- (iv) Substitute the solution of Eq. (2.80), $\phi_1^{(1)}$, for the second term in the RHS of Eq. (2.81) and then solve this for $\phi_2^{(1)}$.

$$\text{Group 2: } -D_2 \nabla^2 \phi_2^{(1)} + (\Sigma_{a,2} + \Sigma_{2 \rightarrow 3}) \phi_2^{(1)} = \frac{\chi_2 P^{(0)}}{k_{eff}^{(0)}} + \Sigma_{1 \rightarrow 2} \phi_1^{(1)} \quad (2.81)$$

- (v) Substitute again the solutions $\phi_1^{(1)}$ and $\phi_2^{(1)}$ from Eqs. (2.80) and (2.81) for the RHS of Eq. (2.82) and then solve this for $\phi_3^{(1)}$.

$$\text{Group 3: } -D_3 \nabla^2 \phi_3^{(1)} + \Sigma_{a,3} \phi_3^{(1)} = \frac{\chi_3 P^{(0)}}{k_{eff}^{(0)}} + (\Sigma_{1 \rightarrow 2} \phi_1^{(1)} + \Sigma_{2 \rightarrow 3} \phi_2^{(1)}) \quad (2.82)$$

(vi) Recalculate k_{eff} by $\phi_1^{(1)}$, $\phi_2^{(1)}$, and $\phi_3^{(1)}$ obtained in (iii) to (v) like Eq. (2.83)

$$k_{eff}^{(1)} = \int_{core} \nu \Sigma_{f,1} \phi_1^{(1)} + \nu \Sigma_{f,2} \phi_2^{(1)} + \nu \Sigma_{f,3} \phi_3^{(1)} dV \quad (2.83)$$

Here, k_{eff} is interpreted as the number of neutrons that will be born in the next generation finally, considering moderation and transport in the whole core, when assuming that one neutron is given as a fission source to the whole core. This is the definition of the effective multiplication factor.

Those solutions are not the correct ones yet because they are based on the initial guesses. The calculations from (iii) to (vi) are iteratively performed until k_{eff} and all of the group fluxes converge. This iterative calculation is known as the *outer iteration* calculation. The outer iteration test for convergence is done by comparing values at an iteration (n) with those at its previous iteration ($n - 1$):

$$\left| \frac{k_{eff}^{(n)} - k_{eff}^{(n-1)}}{k_{eff}^{(n)}} \right| \leq \varepsilon_k \quad (2.84)$$

$$\max_{g, \vec{r}} \left| \frac{\phi_g^{(n)}(\vec{r}) - \phi_g^{(n-1)}(\vec{r})}{\phi_g^{(n)}(\vec{r})} \right| \leq \varepsilon_\phi \quad (2.85)$$

where ε_k and ε_ϕ are the convergence criteria of the effective multiplication factor and neutron flux, respectively.

The relative neutron flux distribution $\phi_g(\vec{r})$ has absolute values due to the thermal power Q of the reactor. The normalization factor A of $\phi_g(\vec{r})$ to an absolute neutron flux distribution $\Phi_g(\vec{r})$ can be determined by

$$\Phi_g(\vec{r}) = A \phi_g(\vec{r}) \quad (2.86)$$

$$Q = \kappa \int_{core} \Sigma_{f,g}(\vec{r}) \Phi_g(\vec{r}) dV = \kappa A \int_{core} \Sigma_{f,g}(\vec{r}) \phi_g(\vec{r}) dV \quad (2.87)$$

where κ is the energy released per fission (about 200 MeV). Finally, the absolute neutron flux distribution for the thermal power can be given as the following.

$$\Phi_g(\vec{r}) = \left(\frac{Q}{\kappa \int_{core} \Sigma_{f,g}(\vec{r}) \phi_g(\vec{r}) dV} \right) \phi_g(\vec{r}) \quad (2.88)$$

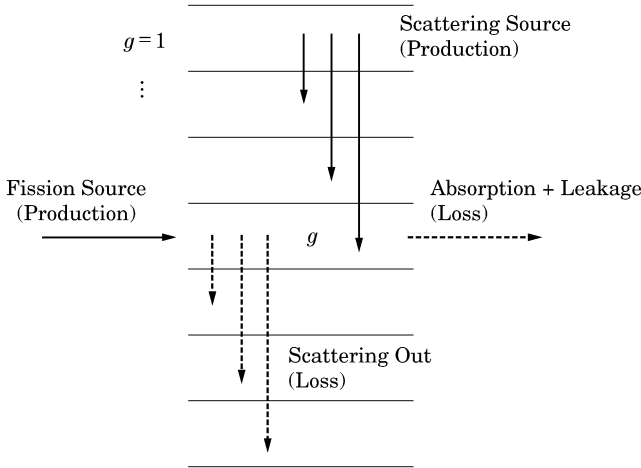


Fig. 2.21 Balance of neutron flux in group g

The distribution of the thermal power within the reactor core is

$$q'''(\vec{r}) = \kappa \sum_g \Sigma_{f,g}(\vec{r}) \Phi_g(\vec{r}) \quad (2.89)$$

which is used as a heat source for the thermal-hydraulic calculation.

A general form of the multi-group diffusion equation in the case of the eigenvalue problem is given by Eq. (2.90), which can be solved in the same way considering the balance between neutron production and loss in group g as shown in Fig. 2.21. It is seen that Eqs. (2.74), (2.75), and (2.76) are also represented by the general form.

$$-D_g \nabla^2 \phi_g + \left(\Sigma_{a,g} + \sum_{g' \neq g} \Sigma_{g \rightarrow g'} \right) \phi_g = \frac{\chi_g}{k_{eff}} \sum_g \Sigma_{f,g} \phi_{g'} + \sum_{g' \neq g} \Sigma_{g' \rightarrow g} \phi_{g'} \quad (2.90)$$

[7] Nodal diffusion method

The finite difference method is widely used in the design calculation of fast reactors, the analysis of critical assembly experiments, and so on. For fast reactors, convergence of the outer iteration is fast due to the long mean free paths of neutrons, and moreover, the nuclear and thermal-hydraulic coupled core calculation is not needed. Hence, the computation speed required for the design calculation can be achieved even with fine meshes in the finite difference method. For conventional LWRs as shown in Fig. 2.22, however, a fine meshing of 1–2 cm is necessary to obtain a high-accuracy solution because the neutron mean free path is short.

For example, a 3D fine meshing of a PWR core of over 30,000 liters leads to a formidable division of several tens of millions of meshes even though

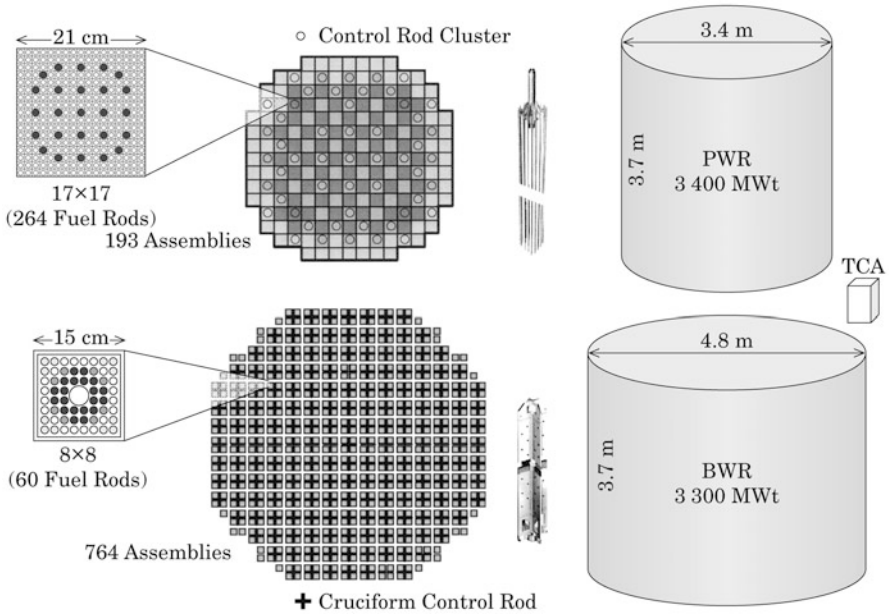


Fig. 2.22 Comparison of conventional LWRs and critical assembly (TCA) in size

excluding the reflector region. Furthermore, the neutron diffusion equation is repeatedly solved in the nuclear and thermal-hydraulic coupled core calculation, core burnup calculation, space-dependent kinetics calculation, and so on. Hence, a calculation using the 3D finite difference method with such a fine meshing is extremely expensive even on a current high-performance computer and therefore it is impractical. The nodal diffusion method [18] was, therefore, developed to enable a high-speed and high-accuracy calculation with a coarse meshing comparable to a fuel assembly pitch (about 20 cm). It is currently the mainstream approach among LWR core calculation methods [19].

The numerical solution of the nodal diffusion method is somewhat complicated and is not discussed here. The main features of the approach are briefly introduced instead.

- (i) Since the coarse spatial mesh (node) is as large as a fuel assembly pitch, the number of unknowns is drastically reduced compared with that of the finite difference method.
- (ii) The 3D diffusion equation in a parallelepiped node (k) is integrated over all directions except for the target direction and then is reduced to a 1D diffusion equation including neutron leakages in its transverse directions. For example, the diffusion equation in the x direction is expressed as

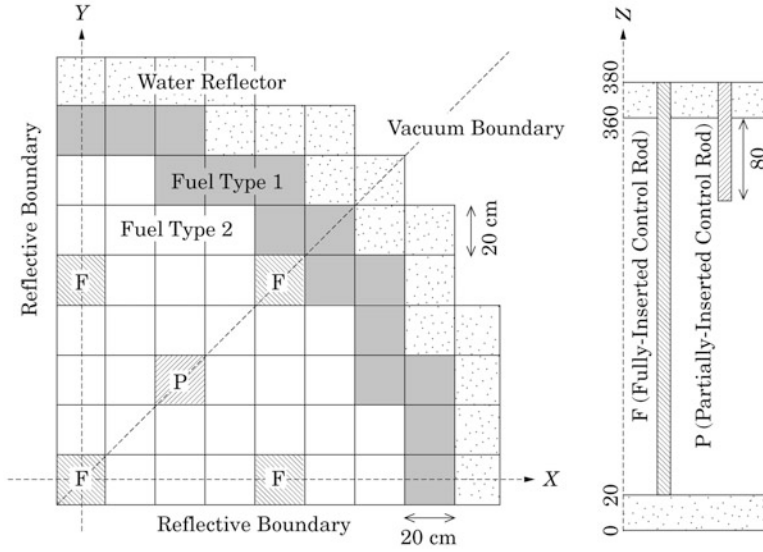


Fig. 2.23 3D benchmark problem of IAEA

$$-D \frac{d^2}{dx^2} \phi_x^k(x) + \Sigma_a \phi_x^k(x) = S_x^k(x) - \left\{ \frac{1}{\Delta_y^k} L_y^k(x) + \frac{1}{\Delta_z^k} L_z^k(x) \right\} \quad (2.91)$$

where Δ_y^k and Δ_z^k are the mesh widths in y and z directions, respectively. $L_y^k(x)$ and $L_z^k(x)$ represent the neutron leakage in each direction. These unknown functions are provided by a second-order polynomial expansion using the transverse leakages of two adjacent nodes.

- (iii) Typical solutions to the 1D diffusion equation of Eq. (2.91) are (a) the analytic nodal method [20] for two-group problems, (b) the polynomial expansion nodal method [18, 21] to expand $\phi_x^k(x)$ into a about fourth-order polynomial, and (c) the analytic polynomial nodal method [22, 23] to expand $S_x^k(x)$ into a second-order polynomial and to express $\phi_x^k(x)$ as an analytic function.

A 3D benchmark problem [24] given by the IAEA as shown in Fig. 2.23 is taken as a calculation example for the suitability of the nodal diffusion method. A PWR core model is composed of two types of fuels and control rods are inserted at five locations of the quadrant inner fuel region. At one location, control rods are partially inserted to 80 cm depth from the top of the core. The meshing effect on the power distribution is relatively large in this case and hence this benchmark problem has been widely employed to verify diffusion codes.

The calculation results using MOSRA-Light code [21] which is based on the fourth-order polynomial nodal expansion method are shown in Fig. 2.24 for two

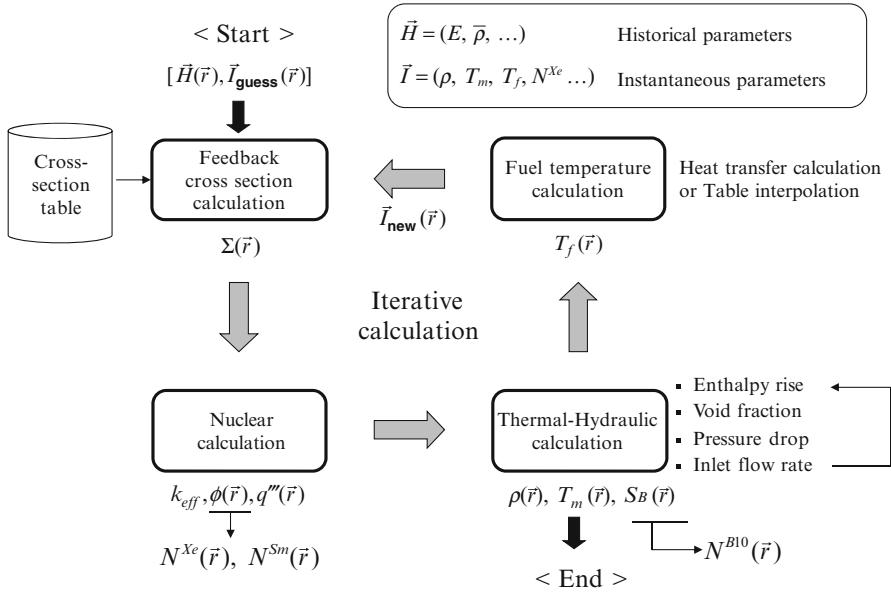


Fig. 2.25 Nuclear and thermal-hydraulic coupled core calculation of LWR

because it is not necessary to solve extra equations. Hence, the nodal diffusion method does not need to have an advantage over the finite difference method for the analysis of fast reactors or small reactors.

[8] Nuclear and thermal-hydraulic coupled core calculation

In the nuclear reactor design calculation, the thermal-hydraulic calculation is performed based on information on the heat generation distribution acquired from the nuclear calculation of the reactor core. In LWRs, the parameters such as moderator temperature, moderator density or void fraction, and fuel temperature obtained from the thermal-hydraulic calculation have a large effect on nuclear characteristics (nuclear and thermal-hydraulic feedback). The nuclear and thermal-hydraulic calculations should be mutually repeated until parameters of both calculations converge. This coupled calculation shown in Fig. 2.25 is referred to as the nuclear and thermal-hydraulic coupled core calculation (hereafter the N-TH coupled core calculation). The procedure of the N-TH coupled core calculation using the macroscopic cross section table prepared from lattice burnup calculations is discussed for a BWR example.

Two types of parameters are used in the coupled calculation. One is historical parameters related to the fuel burnup and the other is instantaneous parameters without a direct relation to it. The historical parameters such as burnup are obtained from the core burnup calculation discussed in the next section. Here it is assumed that all of the historical parameters are known. The macroscopic cross section is first required for the nuclear calculation of the

reactor core. The space and time-dependent macroscopic cross section of a LWR is, for example, represented as Eq. (2.92).

$$\Sigma_{x,g}(\vec{r}, t) = \Sigma_{x,g}(F, R, E, \bar{\rho}, \rho, T_f, T_m, N^{Xe}, N^{Sm}, S_B, f_{CR}, \dots) \quad (2.92)$$

F : fuel type (initial enrichment, Gd concentration, structure type, etc.)

R : control rod type (absorber, number of rods, concentration, structure type, etc.)

E : burnup (GWd/t)

$\bar{\rho}$: historical moderator density (the burnup-weighted average moderator density)

$$\bar{\rho} = \int_0^E \rho dE / \int_0^E dE \quad (2.93)$$

ρ : moderator density (also called the instantaneous moderator density against $\bar{\rho}$) in which the void fraction α in BWRs is calculated from two densities ρ_l and ρ_g in liquid and vapor phases, respectively

$$\rho = \rho_l(1 - \alpha) + \rho_g\alpha \quad (2.94)$$

T_f : fuel temperature (the average fuel temperature in the fuel assembly)

T_m : moderator temperature (the average moderator temperature in the fuel assembly)

N^i : homogenized atomic number density of nuclide i (e.g., ^{135}Xe or ^{149}Sm) for which the atomic number density changes independently of the burnup or the historical moderator density and which has an effect on the core reactivity depending on the operation condition such as reactor startup or shutdown

S_B : concentration of soluble boron (e.g., boron in the chemical shim of PWRs)

f_{CR} : control rod insertion fraction (the fraction of control rod insertion depth: $0 \leq f_{CR} \leq 1$)

These parameters are given as operation conditions, initial guess values, or iterative calculation values, and then the macroscopic cross section for the core calculation is prepared as follows.

- E and R : Use the corresponding macroscopic cross section table.
- E and $\bar{\rho}$: Interpolate the macroscopic cross section table in two dimensions.
- ρ , T_f , and T_m : Use the function fitting Eqs. (2.34), (2.35), and (2.36) based on the branch-off calculation.
- N^i and S_B : Correct the macroscopic cross section in the following equations, using the changes from the condition, in which the homogenized atomic number density was prepared, and the homogenized microscopic cross section:

$$\Sigma_{x,g}(\vec{r}, t) = \Sigma_{0,x,g}(\vec{r}, t) + \Delta N^i(\vec{r}, t) \sigma_{x,g}^i(\vec{r}, t) \quad (2.95)$$

$$\Delta N^i(\vec{r}, t) = N^i(\vec{r}, t) - N_0^i(E, \bar{\rho}) \quad (2.96)$$

where $\Sigma_{0,x,g}(\vec{r}, t)$ is the macroscopic cross section before the correction and $\sigma_{x,g}^i(\vec{r}, t)$ is the homogenized microscopic cross section prepared in the same way as Eq. (2.92). $N_0^i(E, \bar{\rho})$ is the atomic number density homogenized in the lattice burnup calculation and $N^i(\vec{r}, t)$ is the homogenized atomic number density in the core calculation. For example, the atomic number density of ^{135}Xe after a long shutdown is zero and it reaches an equilibrium concentration depending on the neutron flux level after startup. The concentration of soluble boron is similarly corrected changing the homogenized atomic number density of ^{10}B

- f_{CR} : Weight and average the macroscopic cross sections $\Sigma_{x,g}^{\text{In}}$ and $\Sigma_{x,g}^{\text{Out}}$ at control rod insertion and withdrawal respectively with the control rod insertion fraction.

$$\Sigma_{x,g}(\vec{r}, t) = f_{CR} \Sigma_{x,g}^{\text{In}}(\vec{r}, t) + (1 - f_{CR}) \Sigma_{x,g}^{\text{Out}}(\vec{r}, t) \quad (2.97)$$

Since the cross section prepared in the iteration of the N-TH coupled core calculation reflects the feedback of instantaneous parameters, it is hereafter referred to as the *feedback cross section*. The nuclear calculation is performed with the feedback cross section by the nodal diffusion method or the finite difference method and it provides the effective multiplication factor, neutron flux distribution, power distribution, and so on. The distribution of homogenized atomic number density of nuclides such as ^{135}Xe is calculated from necessity. For example, since ^{135}Xe has an equilibrium concentration in a short time after startup as below, it is provided as a homogenized atomic number density used for the correction of microscopic cross section:

$$N^{Xe}(\vec{r}, t) = \left(\gamma^{Xe} \sum_g \Sigma_{f,g}(\vec{r}, t) \Phi_g(\vec{r}, t) \right) / \left(\lambda^{Xe} + \sum_g \sigma_{a,g}^{Xe}(\vec{r}, t) \Phi_g(\vec{r}, t) \right) \quad (2.98)$$

where γ^{Xe} is the cumulative fission yield of ^{135}Xe and λ^{Xe} is the decay constant of ^{135}Xe .

The thermal-hydraulic calculation is performed using the power distribution acquired from the nuclear calculation and gives the instantaneous moderator density ρ and the moderator temperature T_m . A BWR fuel assembly is enclosed in a channel box and the coolant flow inside the assembly is described as a 1D flow in a single channel with a hydraulic equivalent diameter (the “single channel model”). The core is modeled as a bundle of single channels, which are connected at the inlet and outlet, corresponding to each fuel assembly. This is referred to as the 1D multi-channel model. The calculation procedure for ρ and T_m in the 1D multi-channel model is as below.

- (i) The total flow rate at the inlet is constant and the inlet flow rate W_i for channel i is distributed (flow rate distribution). A guessed value is given to W_i if the flow rate distribution is unknown.
- (ii) The axial heat generation distribution $q'_i(z)$ (assembly linear power) of the fuel assembly from the nuclear calculation and the enthalpy at inlet h_i^{IN} are used to calculate the enthalpy rise in each channel.

$$h_i(z) = h_i^{IN} + \frac{1}{W_i} \int_0^z q'_i(z) dz \quad (2.99)$$

- (iii) The physical property values at an arbitrary position $\vec{r}(i, z)$ such as the fluid temperature $T_m(\vec{r})$ and $\rho_l(\vec{r})$ are obtained from the steam table.
- (iv) The void fraction distribution $\alpha(\vec{r})$ is acquired using $q'_i(z)$, $h_i(z)$, physical property values, and some correlations based on the subcooled boiling model. The distribution of the instantaneous moderator density $\rho(\vec{r})$ is calculated using the void fraction distribution.

$$\rho(\vec{r}) = \rho_l \{1 - \alpha(\vec{r})\} + \rho_g \alpha(\vec{r}) \quad (2.100)$$

- (v) The pressure drop ΔP_i by the channel is calculated using the information from (i) to (iv) including $\alpha(\vec{r})$ and correlations on pressure drop
- (vi) The inlet flow rate is determined so that the pressure drop in all channels is equal. A new flow rate distribution $W_i^{new}(z)$ is decided from the flow rate distribution W_i in (i) and the pressure drop ΔP_i in (v).
- (vii) The calculations from (i) to (vi) are repeated until the flow rate distribution is in agreement with the previously calculated one and the pressure drop of each channel is coincident (iterative calculation for flow rate adjustment). $\rho(\vec{r})$ and $T_m(\vec{r})$ at a convergence of the iterative calculation are taken and then the next fuel temperature calculation is done.

In a case such as the space-dependent kinetics calculation, the heat convection and conduction calculation is done using the same iteration approach of the N-TH coupled core calculation and then the temperature distribution in the fuel rod is calculated. In a case such as the steady-state calculation in which operation conditions are limited, it is common to calculate the fuel temperatures at representative linear power and fuel burnup in advance and then interpolate the linear power and burnup obtained from the core calculation into the fuel temperature table to simplify calculation of the fuel temperature $T_f(\vec{r})$.

The calculations mentioned above, the feedback cross section calculation, the nuclear calculation, the thermal-hydraulic calculation, and the fuel temperature calculation, are repeatedly performed until the effective multiplication factor and power distribution reach convergence.

[9] Core burnup calculation

Since the time variation of nuclear characteristics in the core is relatively slow with burnup, the normal N-TH coupled core calculation is carried out using the time-independent equation at each time step as shown in Fig. 2.26.

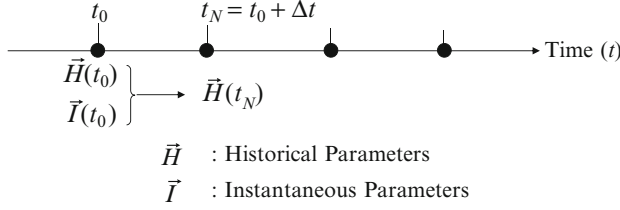


Fig. 2.26 Renewal of historical parameters in core burnup calculation

$\vec{H}(t_0)$ represents the distribution of historical parameters in the core at time t_0 . The burnup $E(\vec{r}, t_0)$ and the historical moderator density $\vec{\rho}(\vec{r}, t_0)$ are the typical historical parameters, and other ones can be used depending on reactor design code. The burnup in conventional LWRs is usually expressed in the unit of (MWd/t), which is measured as the energy (MWd) produced per metric ton of heavy metal initially contained in the fuel. That is, the burnup is the time-integrated quantity of the thermal power.

For the historical moderator density, a spatial distribution of burnup $E(\vec{r}, t_0)$ at time t_0 and a spatial distribution of thermal power density $q'''(\vec{r}, t_0)$ obtained from the N-TH coupled core calculation are considered next. The thermal power density is assumed not to change much through the interval to the next time step ($t_0 \leq t \leq t_0 + \Delta t$). Then, the burnup distribution at time $t_N (= t_0 + \Delta t)$ can be given by

$$E(\vec{r}, t_N) \approx E(\vec{r}, t_0) + C \cdot q'''(\vec{r}, t_0) \Delta t \quad (2.101)$$

where C is a constant for unit conversion.

Next, the distribution of the historical moderator density is recalculated. Since it is the burnup-weighted average value of the instantaneous moderator density, the historical moderator density at time t_N is given by

$$\vec{\rho}(\vec{r}, t_N) \equiv \frac{\int_0^{E_N} \rho(\vec{r}, t) dE}{\int_0^{E_N} dE} = \frac{\int_0^{E_0} \rho(\vec{r}, t) dE + \int_{E_0}^{E_N} \rho(\vec{r}, t) dE}{E(\vec{r}, t_N)} \quad (2.102)$$

where E_0 and E_N are abbreviations of $E(\vec{r}, t_0)$ and $E(\vec{r}, t_N)$, respectively. Here, if the distribution of instantaneous moderator density obtained from the N-TH coupled core calculation at time t_0 remains almost constant during the time interval ($t_0 \leq t \leq t_N$), $\vec{\rho}(\vec{r}, t_N)$ can be expressed as Eq. (2.103).

$$\begin{aligned}\bar{\rho}(\vec{r}, t_N) &\approx \frac{\int_0^{E_N} \rho(\vec{r}, t) dE + \rho(\vec{r}, t_0) \{E(\vec{r}, t_N) - E(\vec{r}, t_0)\}}{E(\vec{r}, t_N)} \\ &= \rho(\vec{r}, t_0) + \{\bar{\rho}(\vec{r}, t_0) - \rho(\vec{r}, t_0)\} \frac{E(\vec{r}, t_0)}{E(\vec{r}, t_N)}\end{aligned}\quad (2.103)$$

Hence, the historical moderator density at the next time step t_N can be calculated using the historical moderator density and the instantaneous moderator density obtained from the N-TH coupled core calculation, at time t_0 . Thus, the core burnup calculation can proceed until the target burnup by renewing the historical parameters with the burnup step.

[10] Space-dependent kinetics calculation

A space-dependent transient analysis for a short time is made using the time-dependent diffusion equation as

$$\begin{aligned}\frac{1}{v_g} \frac{\partial \phi_g(\vec{r}, t)}{\partial t} &= \nabla \cdot D_g(\vec{r}, t) \nabla \phi_g(\vec{r}, t) - \Sigma_{r,g}(\vec{r}, t) \phi_g(\vec{r}, t) \\ &\quad + \sum_{g' \neq g} \Sigma_{g' \rightarrow g}(\vec{r}, t) \phi_{g'}(\vec{r}, t) \\ &\quad + (1 - \beta) \chi_g^p \sum_g \frac{\Sigma_{f,g} \phi_g(\vec{r}, t)}{k_0} + \sum_i \chi_{i,g}^d \lambda_i C_i(\vec{r}, t)\end{aligned}\quad (2.104)$$

where β is the delayed neutron fraction, χ_g^p is the prompt neutron spectrum, and $\chi_{i,g}^d$ is the neutron spectrum of delayed neutron group i . C_i is the precursor concentration of delayed neutron group i and λ_i is its decay constant. Comparison with the normal multi-group diffusion equation [see Eq. (2.90)] shows that the time derivative term in the LHS is added and a different expression of the fission source is given by the fourth and fifth terms of the RHS. Both terms represent the prompt and delayed neutron sources which are classified by time behavior. The precursor concentration balance equation can be given by

$$\frac{\partial C_i(\vec{r}, t)}{\partial t} = \beta_i \sum_{g'} \frac{\Sigma_{f,g'} \phi_{g'}(\vec{r}, t)}{k_0} - \lambda_i C_i(\vec{r}, t) \quad (2.105)$$

For an extremely short time difference of 10^{-4} to 10^{-3} ($t = t^{old} + \Delta t$), the following approximations are introduced.

$$\frac{1}{v_g} \frac{\partial \phi_g}{\partial t} \approx \frac{1}{v_g} \left(\frac{\phi_g - \phi_g^{old}}{\Delta t} \right) \quad (2.106)$$

$$\frac{\partial C_i}{\partial t} \approx \left(\frac{C_i - C_i^{old}}{\Delta t} \right) \quad (2.107)$$

The macroscopic cross section in Eq. (2.104) is the feedback cross section similar to that in the N-TH coupled core calculation. Since Δt is very short, the macroscopic cross section at time t can be substituted by the macroscopic cross section corresponding to the instantaneous parameters at $t = t^{old}$.

$$\Sigma_{x,g}(\vec{r}, t) \approx \Sigma_{x,g}(\vec{r}, t^{old}), T_m(\vec{r}, t^{old}), T_f(\vec{r}, t^{old}), \dots \quad (2.108)$$

Substitution of Eqs. (2.106) and (2.107) into Eqs. (2.104) and (2.105) gives Eq. (2.109).²

$$\begin{aligned} \nabla \cdot D_g \nabla \phi_g - \left(\Sigma_{r,g} + \frac{1}{v_g \Delta t} \right) \phi_g + \sum_{g' \neq g} \Sigma_{g' \rightarrow g} \phi_{g'} \\ + \left\{ 1 - \sum_i \frac{\beta_i}{1 + \lambda_i \Delta t} \right\} \chi_g \sum_{g'} \frac{\Sigma_{f,g'} \phi_{g'}}{k_0} + \left\{ \sum_i \frac{\chi_g \beta_i \lambda_i C_i^{old}}{1 + \lambda_i \Delta t} + \frac{\phi_g}{v_g \Delta t} \right\} \\ = 0 \end{aligned} \quad (2.109)$$

This is in the same form as that of the steady-state multi-group diffusion equation for a fixed-source problem and it can be solved for $\phi_g(\vec{r}, t)$ by the numerical solutions mentioned until now. Then, the thermal-hydraulic calculation is performed and the instantaneous parameters are recalculated, similarly to the steady-state N-TH coupled calculation. The feedback cross section at the next time step is in turn prepared from Eq. (2.108) and the diffusion equation of Eq. (2.109) is solved again. These repeated calculations give the neutron flux distribution and its corresponding thermal power distribution at each time step.

Since it is hard to use a fine time interval less than 10^{-3} s in a practical code for the space-dependent kinetics calculation, a large number of considerations have been introduced for high-speed and high-accuracy calculation within a practical time [19]; two examples are the method to express the time variation in neutron flux as an exponential function and the method to describe the neutron flux distribution as the product of the amplitude component with fast time-variation and the space component with relatively smooth variation (the improved quasi-static method). The fast nodal diffusion method is a general solution in the analysis code for LWRs.

The point kinetics model widely used is in principle based on the first order perturbation theory where it is assumed that the spatial distribution of neutron flux does not change much even though the cross section varies by some external perturbation. Hence, when the neutron flux distribution is considerably distorted due to such an event as a control rod ejection accident, the space-dependent kinetics analysis must accurately predict the time behavior of the reactor.

² For simplicity, it is assumed that $\chi_{i,g}^d = \chi_g$ which is reasonable for the two-group problem.

2.2 Reactor Core, Plant Dynamics and Safety Calculations

Nuclear reactor design and analysis is done with knowledge and data from fundamental fields such as nuclear reactor physics, nuclear reactor kinetics and plant control, nuclear thermal-hydraulic engineering, nuclear mechanical engineering, and nuclear safety engineering. There are various calculation models from simple to detailed, and their selection depends on the purpose. Simple models have the advantage of giving a better understanding of calculation results and physical phenomena, and easy improvement of calculation codes. With today's high computational performance, it is common to use a calculation code based on detailed models from the viewpoint of generic programming. Since the accuracy and application range of calculation results depend on models and data, it is necessary to imagine the physical phenomena and comprehend the validity of the calculation results based on the fundamental knowledge concerning the calculation target.

The nuclear reactor calculation is classified broadly into the reactor core calculation and the nuclear plant characteristics calculation. The former is done to clarify nuclear, thermal, or their composite properties. The latter is done to clarify dynamic and control properties, startup and stability, and safety by modeling pipes and valves of the coolant system, coolant pump, their control system, steam turbine and condenser, etc. connected with the reactor pressure vessel as well as the reactor core.

2.2.1 Reactor Core Calculation

The reactor core calculation is carried out by the N-TH coupled core calculation, presented in the list [8] of Sect. 2.1.5, to evaluate properties in normal operation of the reactor. The concept of core design calculation and the calculation model are discussed here.

[1] Heat transfer calculation in single channel model

Figure 2.27 depicts a 1D cylindrical model to describe one fuel rod and its surrounding coolant with an equivalent flow path. It is called the *single channel model* and it is the basic model used in the core thermal-hydraulic calculation and the plant characteristics calculation. The thermal-hydraulic properties in the core can be calculated on the single channel model where the heat generated from fuel pellets is transferred to coolant which is transported with a temperature rise.

The radial heat transfer model is composed of fuel pellet, gap, cladding, and coolant. The radial heat conduction or convection between those components is considered in each axial region and then the axial heat transport by coolant or moderator is examined. The mass and energy conservation equations and the state equation are solved in each axial region in turn from the top of the upward coolant flow. The momentum conservation equation is also solved to evaluate the pressure drop. The axial heat conduction of the fuel pellet is ignored. This

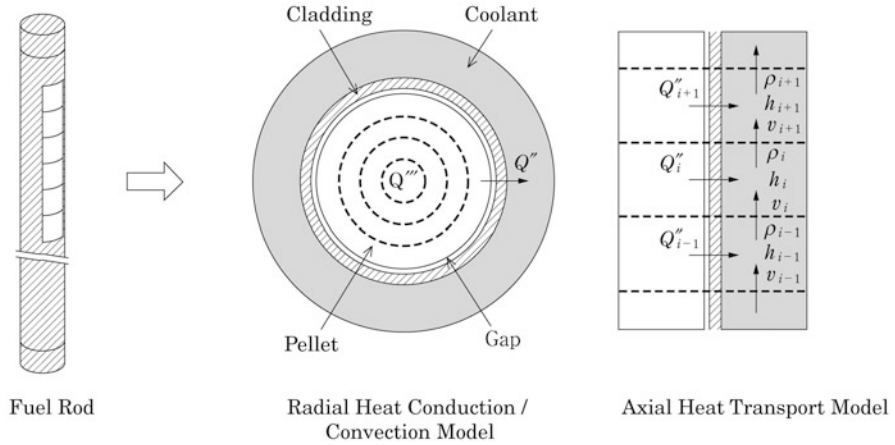


Fig. 2.27 Single-channel heat transfer calculation model

assumption is valid because the radial temperature gradient is several orders of magnitude larger than the axial one.

The difference between the fuel average temperature and the cladding surface temperature is expressed as

$$T_f^{ave} - T_s = \left(\frac{r_f + t_c}{r_f} \right) \left[\frac{r_f}{2k_f} + \frac{1}{h_g} + \frac{t_c}{k_c} \right] q'' \quad (2.110)$$

where,

k_f : average thermal conductivity of pellet (W/m-K)

h_g : gap conductance (W/m²-K)

k_c : thermal conductivity of cladding (W/m-K)

Q'' : heat flux from pellet (W/m²)

r_f : pellet radius (m)

t_c : cladding thickness (m)

T_f^{ave} : pellet average temperature (K)

T_s : cladding surface temperature (K).

The terms inside the RHS square brackets represent the temperature drop in fuel, gap, and cladding, respectively.

The heat transfer from cladding surface to coolant is described by *Newton's law of cooling*

$$q''(r_c) = h_c(T_s - T) \quad (2.111)$$

where,

h_c : heat transfer coefficient between cladding surface and coolant (W/m²-K)

r_c : cladding radius (m)

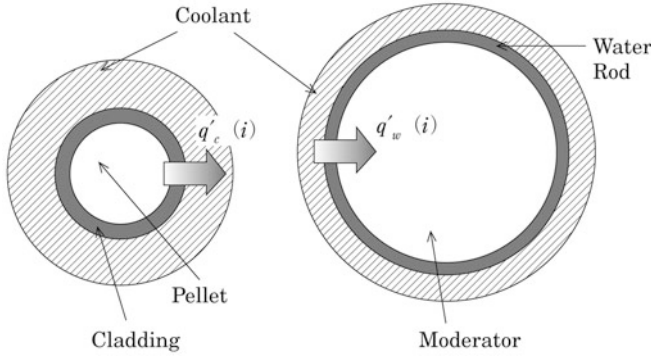


Fig. 2.28 Single-channel thermal-hydraulic calculation model

T_s : cladding surface temperature (K)

T : coolant bulk temperature (K).

The heat transfer coefficient h_c can be evaluated using the *Dittus-Boelter correlation* for single-phase flow and the *Thom correlation* or the *Jens-Lottes correlation* for nucleate boiling.

Water rods are often implemented into fuel assemblies, especially for BWRs. The heat transfer characteristics of the water rod can also be calculated using the single channel model. Figure 2.28 describes the heat transfer calculation model with two single channels of fuel rod and water rod. The heat from coolant is transferred through the water rod wall into the moderator.

The heat transfer of the water rod is also represented by Newton's law of cooling. The temperature difference between the coolant in the fuel rod channel and the moderator in the water rod channel is expressed as

$$T - T_w = \frac{N_f}{N_w} Q'_w \left[\frac{1}{\pi D_w h_{s1}} + \frac{1}{\pi (D_w - 2t_{ws}) h_{s2}} \right] \quad (2.112)$$

where,

T : coolant temperature in fuel rod channel (K)

T_w : moderator temperature in water rod channel (K)

D_w : hydraulic diameter of water rod

h_{s1} : heat transfer coefficient between coolant and outer surface of water rod (W/m²-K)

h_{s2} : heat transfer coefficient between inner surface of water rod and moderator (W/m²-K)

N_f : number of fuel rods per fuel assembly

N_w : number of water rods per fuel assembly

Q'_w : linear heat from coolant to water rod (W/m)

t_{ws} : thickness of water rod (m)

The terms inside of the RHS square brackets represent the heat transfer from the fuel rod channel to the water rod wall and back to the water rod, respectively. Temperature drop due to the water rod wall is ignored in this equation. It is also assumed that the water rod wall is an unheated wall, whereas the cladding is a heated wall. Hence, there is no boiling at the outer surface of the water rod although the outer surface of the water rod wall contacts with two phase coolant. It should be subsequently noted that the application condition of heat transfer correlations is not identical for such a water rod wall.

The thermal conductivity of the fuel pellet depends on temperature and in a BWR fuel, for example, it can be given by

$$k_f = \frac{3824}{402.4 + T_f^{ave}} + 6.1256 \times 10^{-11} (T_f^{ave} + 273)^3 \quad (2.113)$$

where T_f^{ave} and k_f are the average temperature (K) and thermal conductivity (W/m-K) of pellet, respectively. The thermal conductivity is actually a function of pellet density, plutonium containing fraction, burnup, etc. as well as temperature. Since the fission gas release during irradiation causes pellet swelling and hence it also changes the thermal gap conductance with cladding, the fuel behavior analysis code which includes irradiation experiments is required to precisely evaluate the fuel centerline temperature. However, since the fuel centerline temperature at normal operation is far lower than the fuel melting point, it does not need a highly accurately estimate in the reactor core design. In BWR fuel, the fuel centerline temperature at normal operation is limited to about 1,900 °C to prevent excessive fission gas release rate. The temperature drop in the pellet depends not on pellet radius, but linear power density and fuel thermal conductivity. Hence, the linear power density is restricted at normal operation of LWRs.

[2] 3D nuclear and thermal-hydraulic coupled core calculation

In nuclear reactors such as LWRs, in which the coolant serves as moderator, the moderator density varies with temperature change and boiling of coolant, and subsequently the reactivity and reactor power vary. The power distribution also varies with the moderator density change. The heat transfer calculation is performed to evaluate those core characteristics using the heat generation distribution in the core acquired from the nuclear calculation. The nuclear calculation is performed again using the macroscopic cross section changed by the coolant or moderator density distribution obtained in the heat transfer calculation. These calculations are repeated until a convergence. This is the nuclear and thermal-hydraulic coupled core calculation (the N-TH coupled core calculation) mentioned earlier.

A 2D core model cannot precisely handle power and burnup in each part of the core. This usually needs a 3D nuclear calculation, which is combined with the heat transfer calculation in the single channel model for each fuel assembly. Figure 2.29 shows a 3D N-TH coupled core calculation model which is a symmetric quadrant. Since the fuel assembly burnup differs with the power

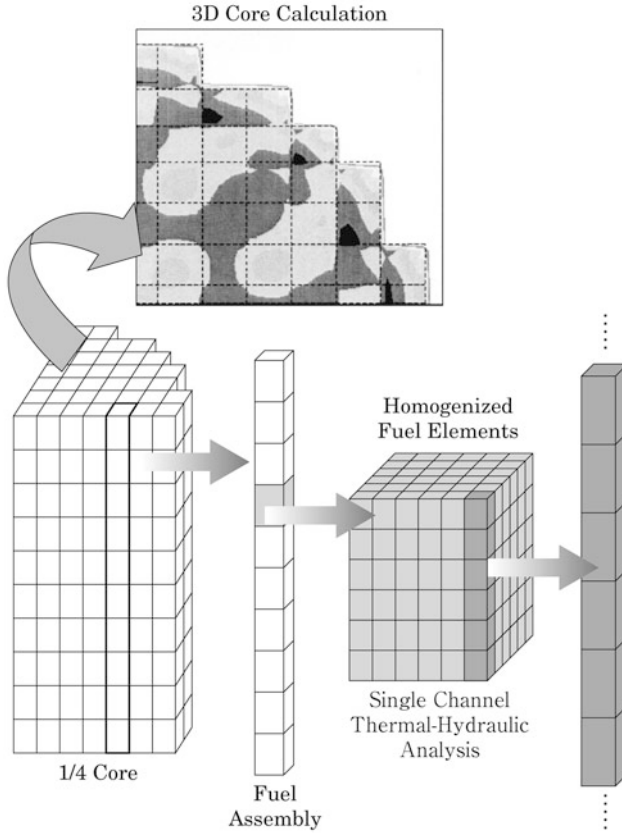


Fig. 2.29 3D nuclear and thermal-hydraulic coupled core calculation model

history at each position, the fuel assembly is axially segmented and the macroscopic cross section at each section is prepared for the core calculation. Each fuel assembly, which consists of a large number of fuel rods, is described as the single-channel thermal-hydraulic calculation model. The heat transfer calculation is carried out with the axial power distribution of each assembly obtained from the nuclear calculation and it provides an axial moderator density distribution.

The N-TH coupled core calculation above is repeatedly continued until it satisfies a convergence criterion and then it gives the macroscopic cross section which is used for calculations such as the core power distribution. This process is repeated at each burnup step and is referred to as the 3D nuclear and thermal-hydraulic coupled core calculation (3D N-TH coupled core calculation). In the practical calculation, as mentioned in Sect. 2.1, the macroscopic cross sections are tabulated in advance with respect to parameters such as fuel burnup and enrichment, moderator density, and so on. Each corresponding cross section is used in the N-TH coupled core calculation.

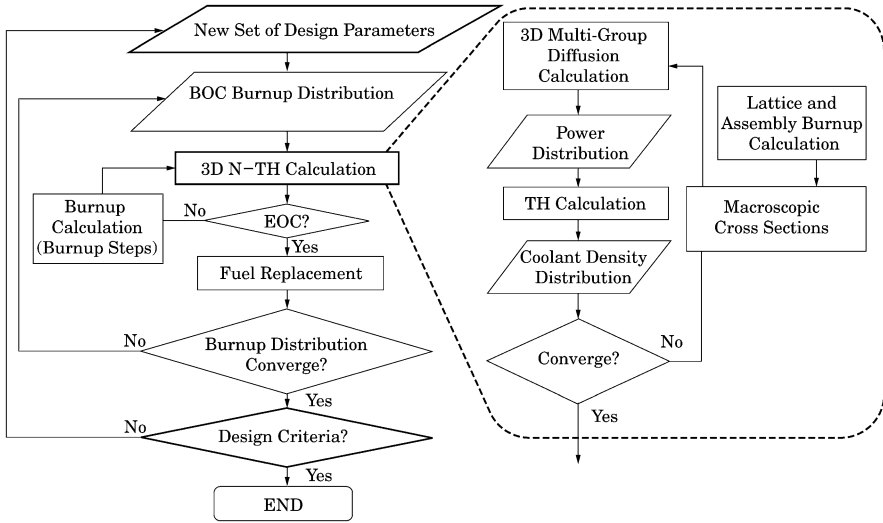


Fig. 2.30 Flow chart of equilibrium code design

Figure 2.30 shows a flow chart of an equilibrium core design using the 3D N-TH coupled core calculation [25]. Macroscopic cross section data are previously prepared from the lattice and/or assembly burnup calculation and then tabulated with fuel burnup and enrichment, moderator density, and so on. The macroscopic cross section is used in the 3D multi-group diffusion calculation to obtain the core power distribution, which is employed again in the thermal-hydraulic calculation.

Usually several different types of fuel assemblies are loaded into the core according to the purpose such as radial power distribution flattening or neutron leakage reduction. In the first operation of a reactor, all fresh fuel assemblies are loaded but they may have several different enrichments of fuel. This fresh core is called the *initial loading core*. After one cycle operation, low reactivity assemblies representing about 1/4 to 1/3 of the loaded assemblies are discharged from the reactor. The other assemblies are properly rearranged in the core considering the burnup distribution and other new fresh ones are loaded.

In the end of each cycle, the core is refueled as in the above way and then the reactor restarts in the next cycle. While such a cycle is being repeated, the characteristics of the core vary but gradually approach equilibrium quantities. When finally the characteristics at $N + 1$ the cycle have little change in comparison with those at the N cycle, the core is called the *equilibrium core*. In certain cases, it shows equilibrium characteristics at N and $N + 2$ cycles and these are also generally referred to as the equilibrium core. By contrast, the core at each cycle is called the “transition core” until it reaches the equilibrium core.

In the equilibrium core design, first a proper burnup distribution of the core is guessed at the beginning of the cycle (BOC), and a control rod and fuel loading pattern is assumed. Then, the N-TH coupled core calculation is performed for one cycle based on the assumed core design with the burnup distribution. After the core calculation, the refueling according to the fuel loading pattern is followed by evaluation of the new burnup distribution at BOC of the next cycle. Such evaluation after one cycle calculation is repeated until the burnup distribution at BOC converges, at which time it is regarded as attaining the equilibrium core.

The core design criteria, such as shutdown margin, moderator density coefficient, Doppler coefficient, fuel cladding temperature, and maximum linear power density, are applied to the equilibrium core. If the equilibrium core does not satisfy the core design criteria, the equilibrium core design is performed again after reviewing fuel enrichment zoning, concentration and number of burnable poison rods, fuel loading and control rod pattern, coolant flow rate distribution, and so on.

A 3D N-TH coupled core calculation is also performed for fuel management such as fuel loading and reloading. In this case, the equilibrium core is searched from an initial loading core. Some fuel assemblies are replaced with new fresh ones after the first cycle calculation and the new core configuration is considered in the next cycle calculation. The calculation procedure is also similar to Fig. 2.30.

It is noted again that operation management such as fuel loading pattern and reloading, and control rod insertion can be considered in the 3D N-TH coupled core calculation. Figure 2.31 shows an example of 3D core power distribution and coolant outlet temperature distribution.

In the core design and operation management, it is necessary to confirm that maximum linear power density (or maximum linear heat generation rate, MLHGR) is less than a limiting value. Figure 2.32 shows variation in MLHGR and maximum cladding surface temperature (MCST) with cycle burnup, which was from a 3D N-TH coupled core calculation for a supercritical water-cooled reactor (SCWR) as an example [26]. The limiting values at normal operation are 39 kW/m and 650 °C respectively in this example. The core calculation was performed according to the fuel loading and reloading pattern as described in Fig. 2.33. It is noted that the third cycle fuel assemblies are loaded in the core peripheral region to reduce neutron leakage (low leakage loading pattern). The control rod pattern is shown in Fig. 2.34.

The 3D N-TH coupled core calculation has been done for BWRs for many years. Since there are not many vapor bubbles in PWRs due to subcooled boiling, the N-TH coupled core calculation has not always been necessary, but it is being employed recently for accuracy improvement.

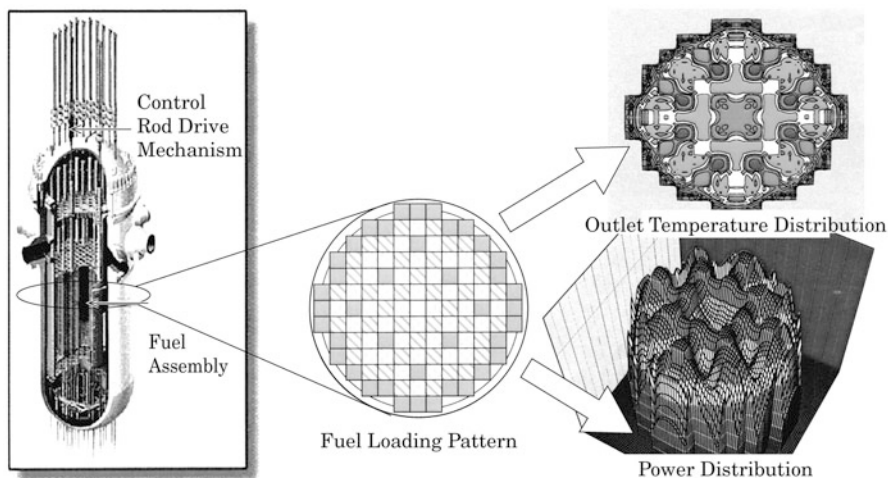


Fig. 2.31 3D core power distribution and coolant outlet temperature distribution

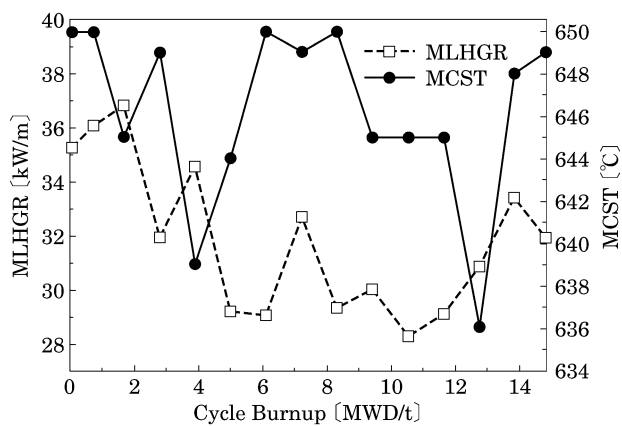


Fig. 2.32 Example of Variation in maximum linear power density and maximum cladding surface temperature with cycle burnup

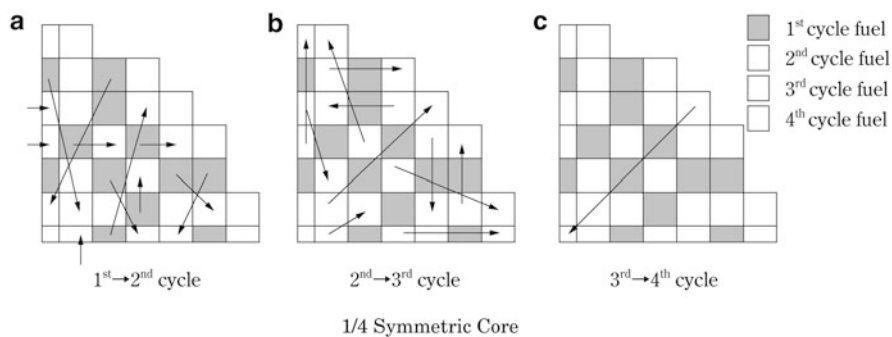


Fig. 2.33 Example of fuel loading and reloading pattern

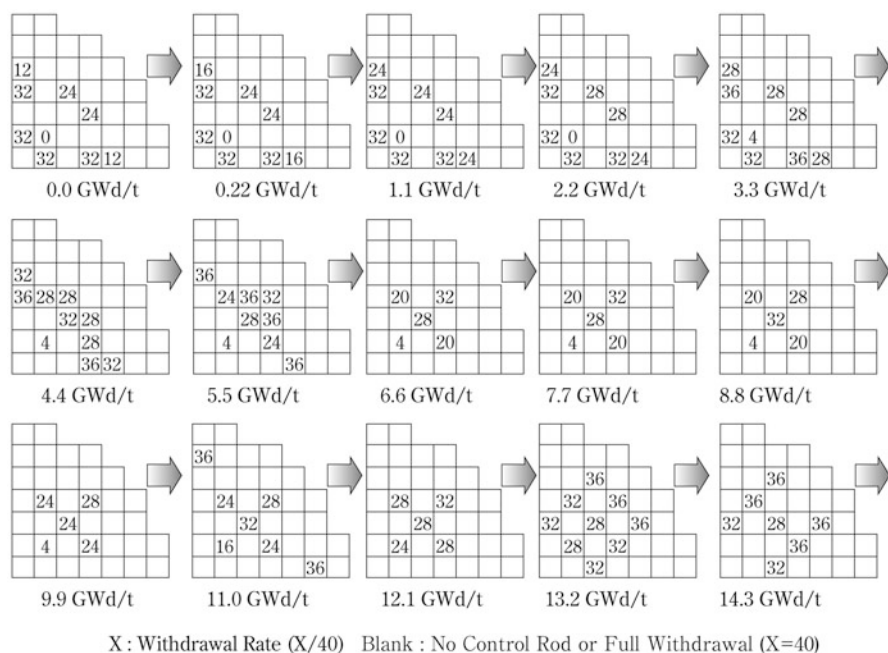


Fig. 2.34 Example of control rod pattern and insertion

In the core calculation, one fuel assembly is modeled not as a bundle of its constituent fuel rods but a homogenized assembly, which is represented as a single channel in the thermal-hydraulic calculation. However, the power of each fuel rod is actually a little different and hence it leads to a different coolant flow rate and a different coolant enthalpy in the flow path (subchannel) between fuel rods. This also causes a difference such as in cladding temperature which is particular to a single-phase flow cooled reactor. The heat transfer analysis for coolant flow paths formed by many fuel rods is called *subchannel analysis*, and it is used in evaluation of cladding temperature in liquid sodium-cooled fast reactors and so on.

In computational fluid dynamics (CFD), the behavior of fluid is evaluated through numerical analysis of the simultaneous equations: Navier–Stokes equations, continuity equation, and in some cases perhaps the energy conservation equation and state equation. It subsequently requires a huge computing time, but a detailed heat transfer analysis can be made. The CFD analysis can be used to calculate a circumferential distribution of fuel rod temperature in a single-phase flow cooled reactor or to analyze detailed fluid behavior inside the reactor vessel and pipes. Figure 2.35 depicts the three heat transfer analysis models mentioned above including the CFD analysis model.

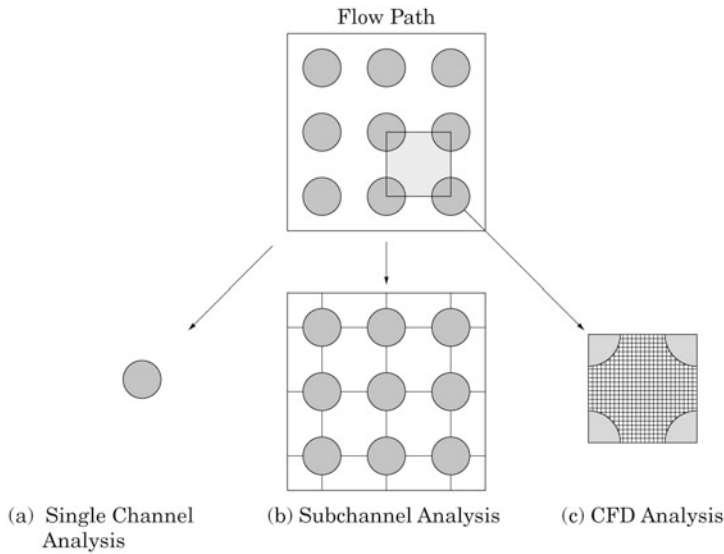


Fig. 2.35 Heat transfer analysis models

2.2.2 Plant Dynamics Calculation

[1] Plant dynamics calculation code

The plant dynamics calculation treats plant control, stability, and response at abnormal transients and accidents. A simple model for heat transfer calculation in a plant is the node junction model as shown in Fig. 2.36 [27]. In the node junction model, reactor components are represented as 1D nodes and connected; the connected items include core, upper and lower plena, downcomer (inlet coolant flows down the downcomer region which is placed between the core and reactor pressure vessel), main feedwater and main steam lines, valves, etc. The node junction calculation begins from an upstream node based on mass and energy conservation laws. The momentum conservation law is also considered for pressure drop and flow rate distribution calculations. In the case of Fig. 2.36, for example, the core is described with two single channel models at average and maximum power. The core design calculation is performed at steady state as mentioned before, but a transient single channel model is used in the plant dynamics calculation.

A transient radial heat conduction in fuel can be expressed as

$$\frac{\partial}{\partial t} (\rho_f C_p T_f) = \frac{1}{r} \frac{\partial}{\partial r} \left(r k_f \frac{\partial T_f}{\partial r} \right) + q''' \quad (2.114)$$

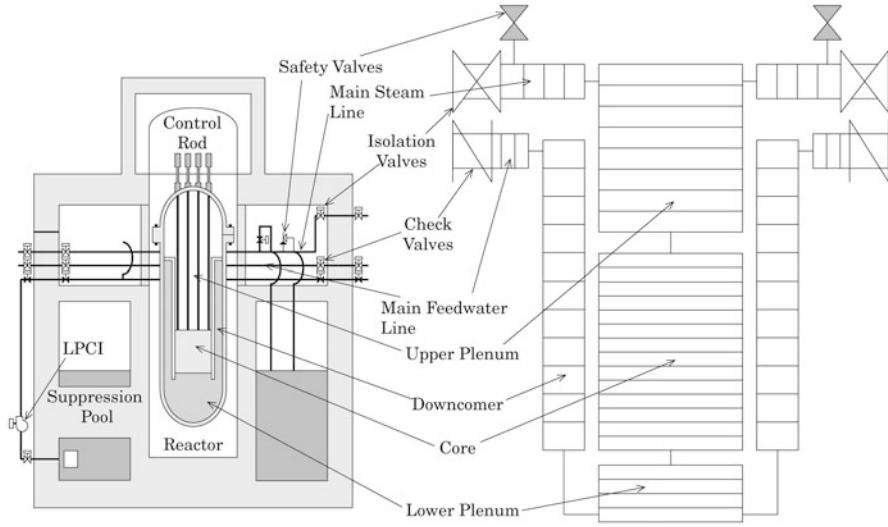


Fig. 2.36 Node junction model

where,

C_p : specific heat of pellet (J/kg-K)

k_f : thermal conductivity of pellet (W/m-K)

q^m : power density (W/m³)

r : radial distance (m)

T_f : pellet temperature (K)

ρ_f : pellet density (kg/m³).

The heat transfer from cladding outer surface to coolant is evaluated by Newton's law of cooling. A proper heat transfer coefficient should be used considering flow regime and temperature, pressure, etc.

Plant dynamics analysis codes are constructed with the node junction model and the following reactor kinetics model. The simplest kinetics model is the point reactor kinetics model (point reactor approximation) as

$$\frac{\partial n(t)}{\partial t} = \frac{\Delta\rho - \beta}{\Lambda} n(t) + \sum_{i=1}^6 \lambda_i C_i(t) \quad (2.115)$$

$$\frac{\partial C_i(t)}{\partial t} = \frac{\beta_i}{\Lambda} n(t) - \lambda_i C_i(t) \quad (i=1 \sim 6)$$

$$\Delta\rho = \Delta\rho(T_f^{ave}, \rho_{mod})$$

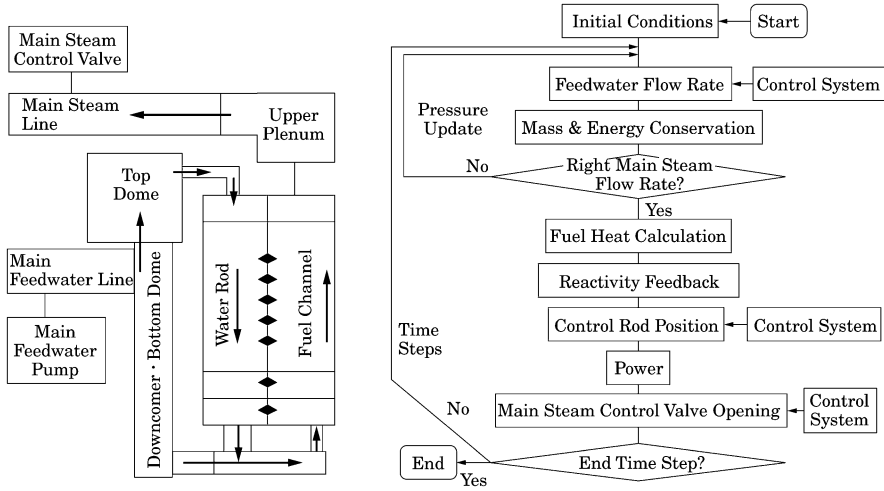


Fig. 2.37 Plant dynamics analysis model and calculation flow chart

where,

$n(t)$: number of neutrons

$C_i(t)$: number of delayed neutron precursor for group i

t : time

β_i : fraction of delayed neutron group i

$$\beta: \sum_{i=1}^6 \beta_i$$

$\Delta\rho$: reactivity

Λ : prompt neutron generation time (s)

λ_i : decay constant of precursor of delayed neutron group i (s^{-1})

$T_f^{ave}(t)$: average fuel temperature (K)

$\rho_{mod}(t)$: moderator density (g/cm^3).

The reactivity feedback of fuel temperature (Doppler effect) and moderator density is applied to the point reactor kinetics equations. Even though large power reactors such as LWRs show space-dependent kinetic characteristics, the reactivity feedback effect can be expressed with the point reactor approximation using a space-dependent weight function (adjoint neutron flux).

Figure 2.37 shows an example of a node junction model in a plant dynamics analysis code and its calculation flow chart. This model describes coolant flow which is fed to the water moderation rods through the top dome of the reactor vessel for a supercritical water-cooled thermal reactor (Super LWR) [28, 29].

The mass, energy, and momentum conservation equations used in the node junction model are a time-dependent form of the single-channel

thermal-hydraulic model in the core design. In the case of single channel, single phase, and one dimension, the mass conservation equation is given by Eq. (2.116)

$$\frac{\partial \rho}{\partial t} + \frac{\partial(\rho u)}{\partial z} = 0 \quad (2.116)$$

and the energy conservation equation is given by Eq. (2.117).

$$\frac{\partial(\rho h)}{\partial t} + \frac{\partial(\rho u h)}{\partial z} = \frac{P_e}{A} q'' \quad (2.117)$$

The momentum conservation equation is expressed as

$$-\frac{\partial P}{\partial z} = \frac{\partial(\rho u)}{\partial t} + \frac{\partial(\rho u^2)}{\partial z} + \rho g \cos \theta + \frac{2f}{D_h} \rho u^2 \quad (2.118)$$

and the state equation is

$$\rho = \rho(P, h) \quad (2.119)$$

where,

t : time (s)

z : position (m)

ρ : coolant density (kg/m³)

u : fluid velocity (m/s)

h : specific enthalpy (J/kg)

q'' : heat flux at fuel rod surface (W/m²)

A : flow area of fuel channel (m²)

P_e : wetted perimeter of fuel rod (m)

P : pressure (Pa)

g : gravitational acceleration

D_h : hydraulic equivalent diameter of fuel channel (m)

Re: Reynolds number

θ : vertical angle of fuel channel

f : frictional coefficient

for example, $f = 0.0791 \times \text{Re}^{-0.25}$ (Blasius equation).

In the case of a water rod, the energy transferred to the water rod should be considered in the energy conservation equation of the fuel rod cooling channel. In the case of light water, the steam tables of the Japan Society of Mechanical Engineers (JSME) or the American Society of Mechanical Engineers (ASME) can be used in the state equation of the coolant.

The following introduce heat transfer coefficients for water-cooled reactors. In a single-phase turbulent flow, for example, the heat transfer coefficient can be obtained from the Dittus-Boelter correlation

$$h = 0.023 \left(\frac{k}{D_e} \right) (Pr)^{0.4} \left(\frac{GD_e}{\mu} \right)^{0.8} \quad (2.120)$$

where,

D_e : hydraulic equivalent diameter (m)

G : mass flux ($\text{kg/m}^2\text{-s}$)

h : heat transfer coefficient ($\text{W/m}^2\text{-K}$)

k : thermal conductivity (W/m-K)

Pr : Prandtl number

μ : viscosity coefficient (Pa-s).

If nucleate boiling occurs, the heat transfer for PWR can be described by the Thom correlation

$$h = \frac{1}{dT} \left(\frac{\Delta T_{sat} e^{P/8.6}}{0.022} \right)^2 \quad (2.121)$$

where,

h : heat transfer coefficient ($\text{W/m}^2\text{-K}$)

P : pressure (MPa)

dT : temperature difference between wall surface and fluid (K)

ΔT_{sat} : wall temperature elevation above saturation temperature (K)

and it is applied for the range of

pressure: 5.2–14.0 MPa

mass flux: 1,000–3,800 $\text{kg/m}^2\text{-s}$

heat flux: 0–1600 kW/m^2 .

The Jens-Lottes correlation can be used for BWRs.

If there is a thin liquid film in annular flow with a high steam quality, for example, the heat transfer to a vertical upward water flow can be represented by the *Schrock-Grossman correlation*

$$h = (2.50)(0.023) \left(\frac{k_f}{D_e} \right) (Pr_f)^{0.4} \left[\frac{GD_e(1-X)}{\mu_f} \right]^{0.8} \left(\frac{1}{X_{tt}} \right)^{0.75} \quad (2.122)$$

$$\frac{1}{X_{tt}} = \left(\frac{X}{1-X} \right)^{0.9} \left(\frac{\rho_f}{\rho_g} \right)^{0.5} \left(\frac{\mu_g}{\mu_f} \right)^{0.1}$$

where,

D_e : hydraulic equivalent diameter (m)

G : mass flux ($\text{kg/m}^2\text{-s}$)

h : heat transfer coefficient (W/m²-K)
 k_f : thermal conductivity of water (W/m-K)
 Pr_f : Prandtl number of water
 X : steam quality
 ρ_f : water density (kg/m³)
 ρ_g : steam density (kg/m³)
 μ_f : viscosity coefficient of water (Pa-s)
 μ_g : viscosity coefficient of steam (Pa-s)

and it is applied for the range of

pressure: 0.3–3.5 MPa
 mass flux: 240–4,500 kg/m²-s
 heat flux: 190–4,600 kW/m².

In the post-dryout region of BWRs, namely, the steady-state film boiling state of mist flow where steam flow is accompanied with liquid droplets, for example, the heat transfer can be described by the *Groeneveld correlation*.

$$h = 0.00327 \left(\frac{k_g}{D_e} \right) (Pr_{v,w})^{1.32} \left[\left(\frac{GD_e}{\mu_g} \right) \left(X + \frac{\rho_g}{\rho_f} (1 - X) \right) \right]^{0.901} Y^{-1.50} \quad (2.123)$$

$$Y = \max \left[1 - 0.1(1 - X)^{0.4} \left(\frac{\rho_f}{\rho_g} - 1 \right)^{0.4}, 0.1 \right]$$

where,

h : heat transfer coefficient (W/m²-K)
 k_g : thermal conductivity of saturated steam (W/m-K)
 $Pr_{v,w}$: Prandtl number of steam at wall surface
 D_e : hydraulic equivalent diameter (m)
 G : mass flux (kg/m²-s)
 μ_g : viscosity coefficient of steam (Pa-s)
 X : steam quality
 ρ_f : water density (kg/m³)
 ρ_g : steam density (kg/m³)

[2] Plant control

The plant dynamics analysis covers the plant control system. Figure 2.38 presents the plant control system of a SCWR as an example [27]. Typical control systems of LWRs are actually more complex, but they are based on the concept below. The plant control system of nuclear power plants uses *proportional-integral-derivative (PID) control* which is widely used in the control system of other types of practical plants as well.

Composition of the plant control system is based on similar existing plant control systems and its parameters are determined using plant dynamics analysis codes using the procedure below.

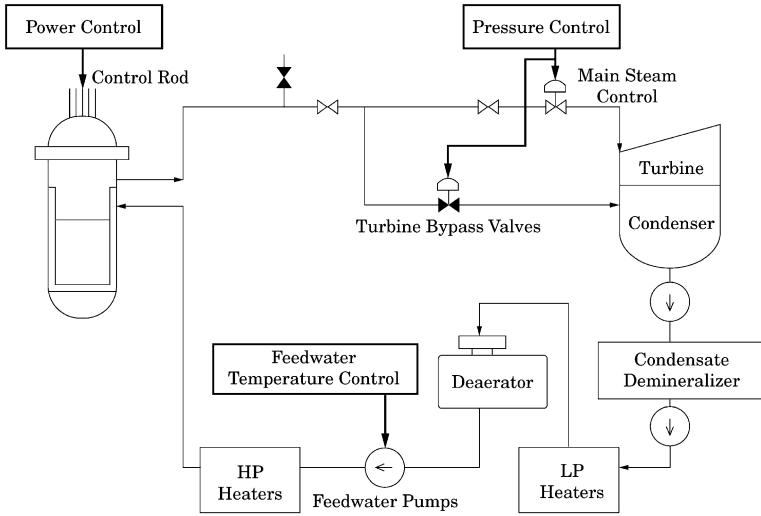


Fig. 2.38 Plant control system (supercritical water-cooled reactor)

- ① Investigate responses to external disturbances without control system, and decide what state variables (e.g., power) to control and how to control them (e.g., by control rod) according to their sensitivities.
- ② Design a control system.
- ③ Confirm responses to the external disturbances under the control system.

For example, in the case of reducing feedwater flow rate, changing control rod position, inserting a reactivity, or closing main steam control valves, variations in main steam temperature, power, or pressure are investigated for each case using plant dynamics analysis codes. In Fig. 2.38, the main steam temperature is controlled by regulating feedwater flow rate, the reactor power by control rods, and the main steam pressure by main steam control valves considering highly sensitive parameters.

Figure 2.39 shows the power control system by control rods. This control system is governed by a proportional controller which decides a control rod drive speed in proportion to the deviation between actual power and power setpoint. Control rods are driven at a maximum speed for a deviation larger than a constant value b .

Figure 2.40 represents the main steam temperature control system which is driven by a proportional-integral (PI) controller after a lead compensation for time-lag of a temperature sensor. The PI control parameter values are determined for stable and fast-convergence responses through fine tuning of the integral gain with a little change of the proportional gain.

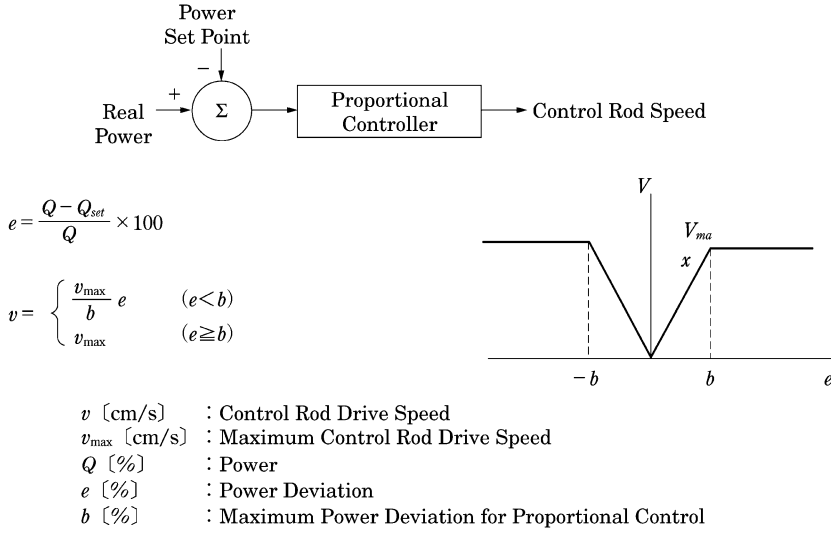


Fig. 2.39 Power control system

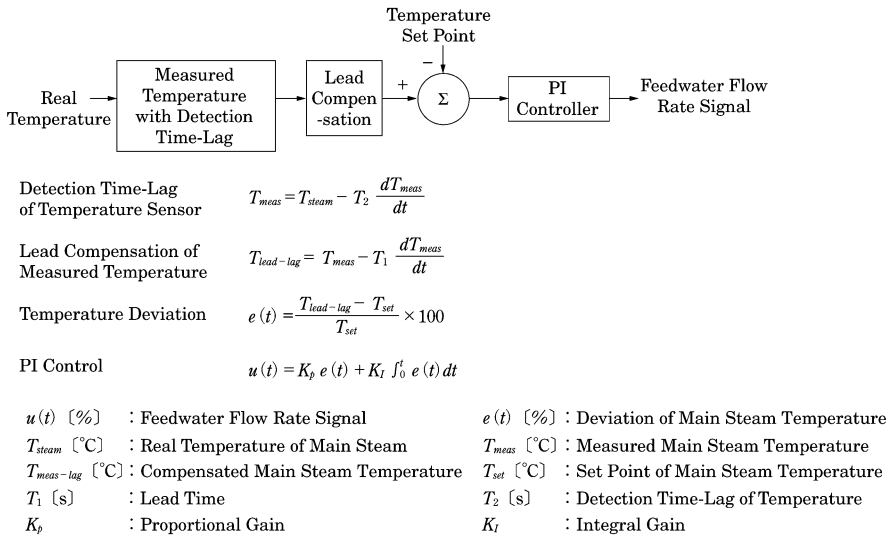
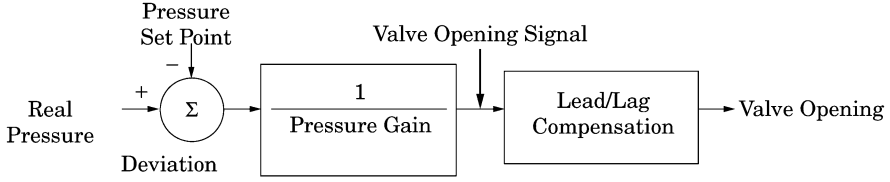


Fig. 2.40 Main steam temperature control system

Figure 2.41 shows the pressure control system which controls valve opening by converting the deviation from the pressure setpoint into a valve opening signal with lead/lag compensation. The control parameter value is determined for a stable convergence response from investigation of a time variation in the main steam pressure with a little change of the pressure gain.



$$V_{demand}(t) = 100 - \frac{P - P_{set}}{K}$$

$$V(t) = T_1 \frac{dV_d}{dt} - T_2 \frac{dV}{dt}$$

- P [MPa] : Turbine Inlet Pressure
 P_{set} [MPa] : Set Point of Turbine Inlet Pressure
 V [%] : Opening of Main Steam Control Valve
 T_1 [s] : Lead Time
 T_2 [s] : Lag Time
 K [MPa] : Pressure Gain
 V_{demand} [%] : Opening Signal of Main Steam Control Valve

Fig. 2.41 Pressure control system

After all control systems are set up, the plant behavior with external disturbances of power, pressure, and flow rate is analyzed using the plant dynamics analysis code until finally stable and fast convergence is confirmed.

[3] Plant startup

Since the plant startup and stability show a slow behavior change over a long time, the balance of plant (BOP) such as the turbine system is included in the calculation model of plant dynamics calculation codes. Figure 2.42 shows an example of the calculation model for a SCWR [28]. The BOP can be modeled as properly describing mass and energy conservation and plant time behavior without a detailed embodiment. The reactor core is represented as a single channel model in the figure, but it can be described by two single channels, i.e. average and hot channels.

The following are models for pressure change in inlet orifice, feedwater pump, feedwater pipe, and outlet valve used in the ex-core circulation system.

$$\text{Orifice Model: } \Delta P = \zeta \frac{\rho u^2}{2}$$

$$\text{Feedwater pump model: } \delta P = C_{pump} \delta u$$

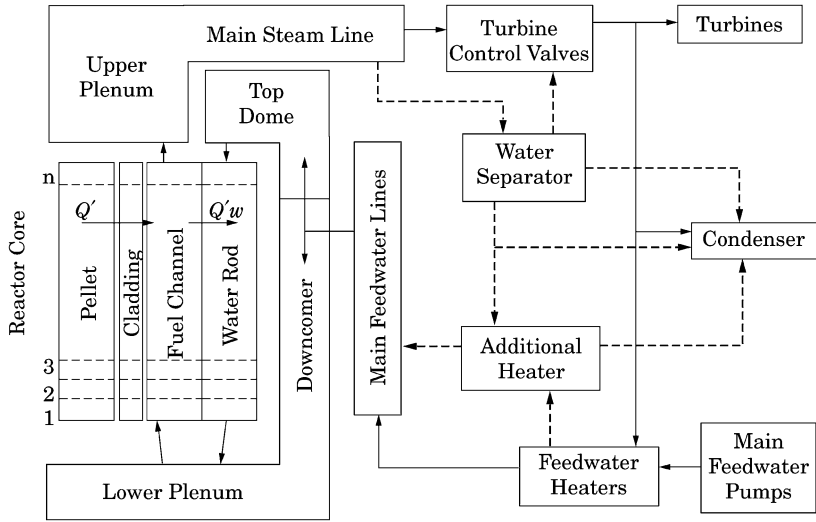


Fig. 2.42 Calculation model for plant startup and stability analysis

$$\text{Feedwater line model: } -\frac{dP}{dz} = \frac{d}{dt} \rho u + \frac{d}{dz} \rho u^2 + \frac{2f}{D} \rho u^2$$

$$\text{Valve model: } \Delta P = \zeta \frac{\rho u^2}{2}$$

P : pressure (Pa)

ΔP : pressure drop (Pa)

δP : pressure change in pump (Pa)

ζ : orifice or valve pressure drop coefficient

ρ : coolant density (kg/cm^3)

u : fluid velocity (m/s)

δu : fluid velocity change in pump

C_{pump} : pressure drop coefficient of pump

z : position (m)

t : time (s)

f : friction pressure drop coefficient

D : diameter of feedwater pipe (m)

The plant startup procedure is established to satisfy constraints at startup using the calculation models above. The constraints at startup depend on reactor type: for example, maximum cladding surface temperature for SCWRs; restrictions in heat flux, various safety parameters, and pump cavitation for LWRs; restrictions of vapor fraction in main steam for direct-cycle reactors. There are also restrictions from thermal stress to temperature rise of the reactor vessel.

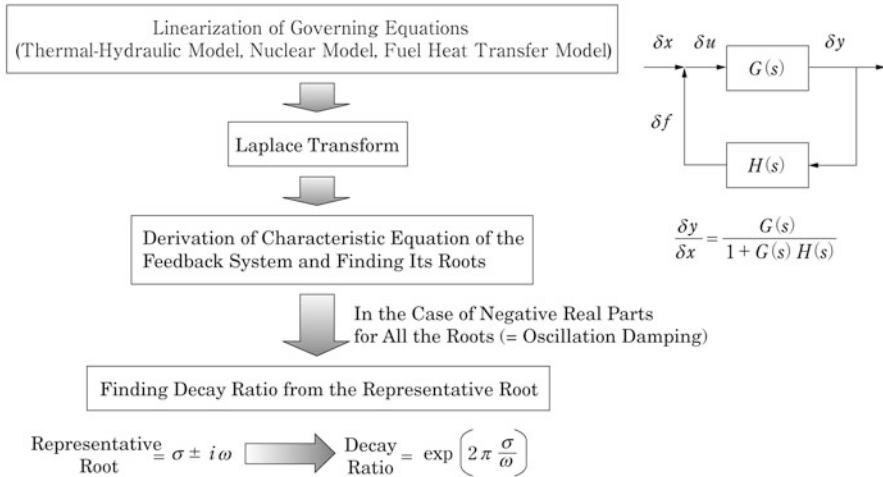


Fig. 2.43 Procedure of linear stability analysis

[4] Reactor stability analysis

In the reactor stability analysis, first governing equations are established for normal and perturbed values of state variables from the plant dynamics codes and then the governing equations are linearized for the perturbed one. The equations are converted into a frequency domain by the Laplace transform and analyzed there. This is referred to as *linear stability analysis* and the procedure for it in the frequency domain is shown in Fig. 2.43.

In the figure, the system transfer function (closed-loop transfer function) is defined with the open-loop transfer functions, $G(s)$ and $H(s)$. The system stability is characterized by the poles of the transfer function (the roots of the characteristic equation in its denominator) and described by the decay ratio. The concept and the stability criteria are given in Fig. 2.44. For the system to be stable with damping, all the roots of the characteristic equation must have negative real parts. The decay ratio, which is defined as the ratio of two consecutive peaks of the impulse response of the oscillation for the representative root (the root nearest to the pole axis), depends on the calculation mesh size. The decay ratio is determined by extrapolation to zero mesh size following calculations with different mesh size.

The following should be considered in the stability analysis of nuclear reactor design.

- Channel stability: This is thermal-hydraulic stability of the fuel cooling channel.
- Core stability: This is the nuclear and thermal-hydraulic coupled stability where the whole core power (neutron flux) regularly oscillates as a fundamental mode due to the moderator density feedback

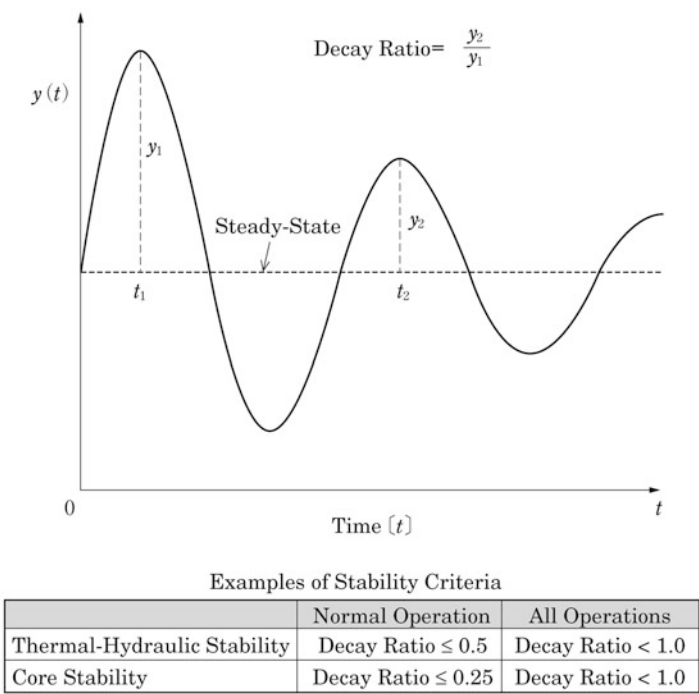


Fig. 2.44 Decay ratio and stability criteria

- (iii) Regional stability: This is a kind of core stability and the neutron flux of each region oscillates as a high-order mode by reciprocally going up and down.
- (iv) Plant stability
- (v) Xenon stability (Xe spatial oscillation): This is a function of accumulation and destruction of FP Xe, and spatial change of neutron flux

The channel stability is thermal-hydraulic stability of single coolant channel in the core. The core stability is the nuclear and thermal-hydraulic coupled stability where the whole core power (neutron flux) regularly oscillates as a fundamental mode due to the moderator density feedback. The regional stability is a kind of core stability and the neutron flux of each region oscillates as a high-order mode by reciprocally going up and down. These three stabilities are inherent characteristics of nuclear reactors with a large change in moderator density in the core such as BWRs, and hence they are evaluated by the frequency-domain stability analysis. The plant stability is the stability of plant system including its control system and is evaluated by time-domain analysis using a plant dynamics analysis code. Xenon spatial oscillation is caused by accumulation and destruction of Xenon-135, and spatial change of neutron flux. The xenon stability is analyzed by the production and destruction equation of Xenon-135.

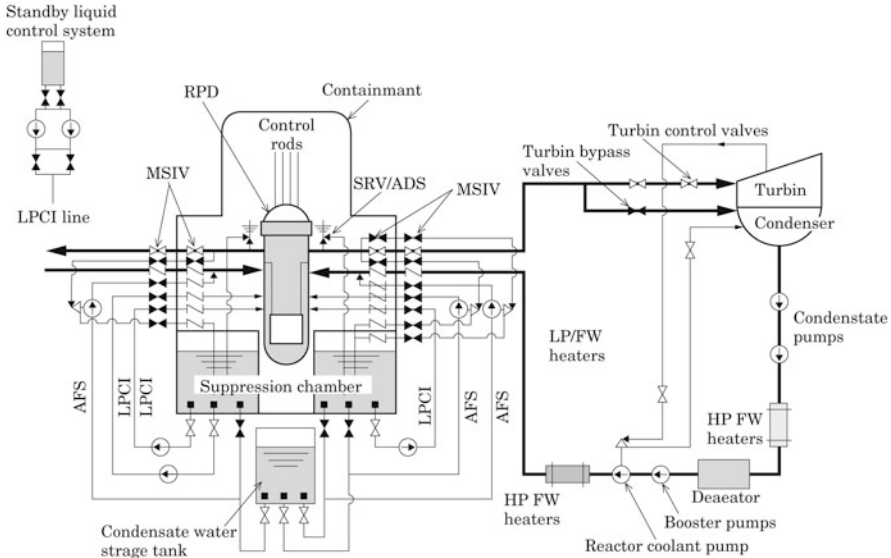


Fig. 2.45 Plant and safety system (SCWR)

2.2.3 Safety Analysis

[1] Analysis of abnormal transients and design based accidents

In the safety analysis of nuclear power plants, safety system models and scenarios of abnormalities are implemented into the plant dynamics calculation code. Abnormal events are classified into abnormal transients and design basis accidents depending on the initial event frequency, namely, high and low frequencies respectively.

For examples, Fig. 2.45 describes the plant system of a SCWR with the safety system and Fig. 2.46 shows the calculation model of its safety analysis code [27, 29].

The SCWR is a direct steam cycle system and its safety system is similar to that of BWRs. Safety relief valves (SRVs) and an automatic depressurization system (ADS) are installed into the main steam lines. Turbine bypass valves are used to dump the main steam to the condenser at a sudden closure of the main steam control valves. This is made in a manner to prevent damage to the turbine from over-rotation by a turbine load loss due to a breakdown of the electric transmission system. The high-pressure auxiliary feedwater system (AFS, high-pressure coolant injection system) is equipped to maintain coolant supply at an abnormal event of the main feedwater system. The low pressure coolant injection (LPCI) system is prepared to flood and cool the core after reactor depressurization at a loss of coolant accident (LOCA). The water is fed from the suppression chamber or condensate water storage tank. The LPCI system also

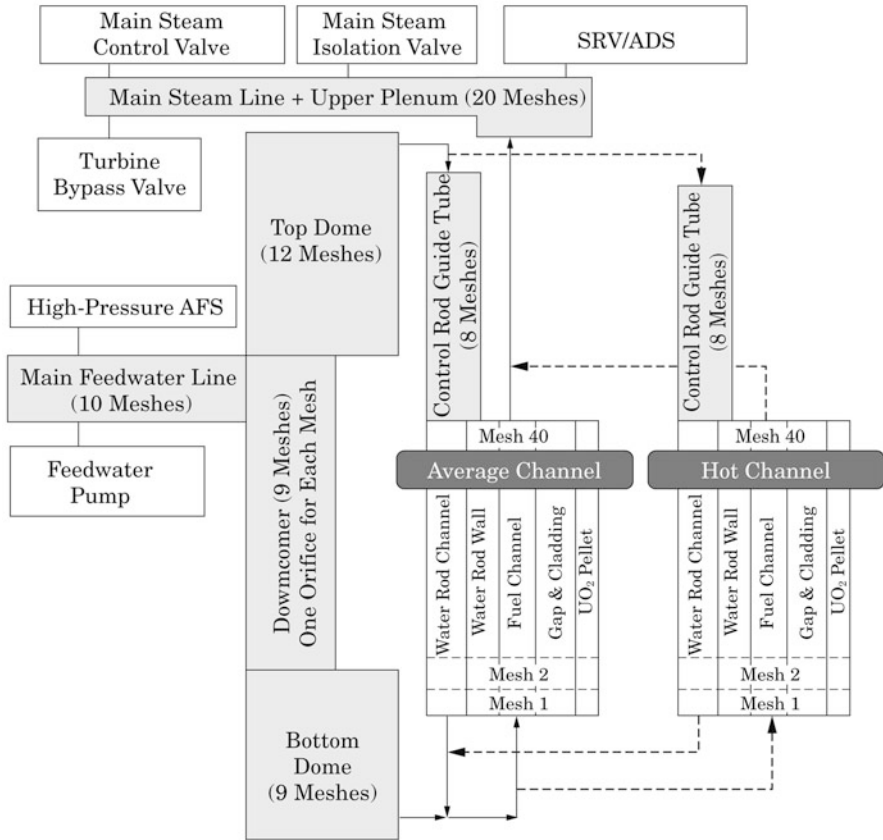


Fig. 2.46 Calculation model for abnormal transient and accident analysis

has the function of residual heat removal (RHR) after reactor shutdown. The boric acid injection system (standby liquid control system, SLC system) is provided for backup shutdown.

Figure 2.46 models main steam control valves (turbine control valves), SRVs, turbine bypass valves, AFS, reactor coolant pump (RCP), and so on. The core is modeled by average and hot channels. Since abnormal events for safety analysis are often relatively short-term ones, heat removal models including the turbine system are not always necessary. The calculation model in the figure does not comprise safety systems for LOCA analysis such as the LPCI. General-purpose safety analysis codes have models to handle those systems.

[2] Loss of coolant accident

LOCA analysis is composed of two parts: blowdown phase and reflood phase. As an example of SCWR, the blowdown analysis model is shown in Fig. 2.47 in which valves and systems able to simulate cold-leg break and hot-leg break are implemented into the abnormal transient and accident analysis model of Fig. 2.46.

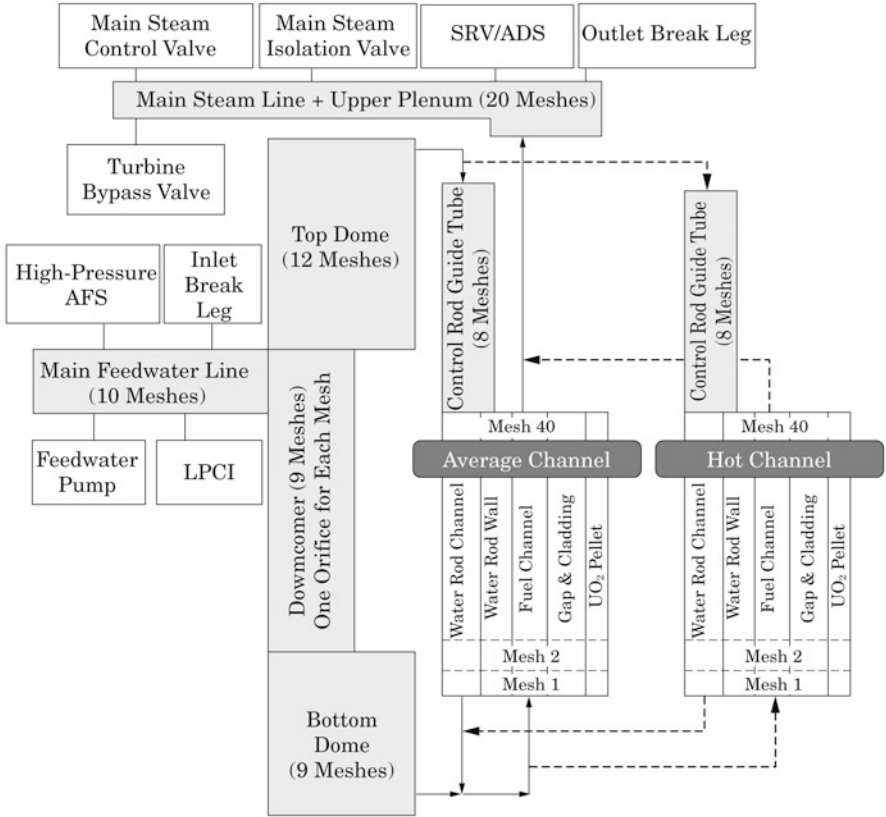


Fig. 2.47 Calculation model for LOCA blowdown analysis

The reflood phase can be analyzed by modeling the LPCI in the calculation code as shown in Fig. 2.48. In the practical analysis of plant safety, general-purpose codes are used to describe more detailed models and to calculate the blowdown and reflood phases as one body.

2.2.4 Fuel Rod Analysis

[1] Fuel rod integrity

The principle role of fuel rod cladding is to confine radioactive FPs and to prevent contamination of the coolant system; therefore an assurance of fuel rod integrity is important for reactor design and safety.

When an abnormal transient event occurs in a nuclear plant with a frequency of more than once during the plant life time, the safety criterion is associated with whether the core can return to the normal operation without core damage

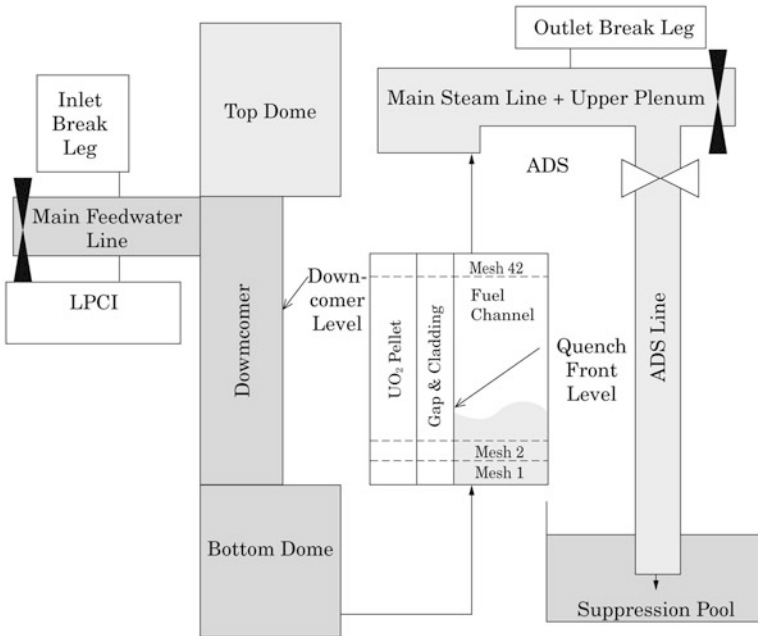


Fig. 2.48 Calculation model for LOCA reflooding analysis

after the plant is stabilized. Thus, fuel rods are required to keep their integrity during abnormal transients (anticipated operational occurrences) as well as normal operation.

The criteria for fuel rod integrity differ somewhat between BWRs and PWRs because of different operating conditions. Fuel rods are designed generally based on the following criteria [25, 27].

- (i) Average circumferential plastic deformation of fuel cladding < 1 %
- (ii) Fuel centerline temperature < Pellet melting point (PWR)
- (iii) No overpressure within fuel rod
- (iv) Allowable stress of fuel rod cladding
- (v) Cumulative damage fraction < 1

The overall fuel rod integrity is evaluated further in cladding corrosion and hydriding, pellet cladding interaction (PCI), cladding creep rupture, rod fretting wear, cladding bending, and irradiation growth of the fuel rod and assembly.

The fuel damage criteria and allowable limits of BWRs and PWRs are given in Table 2.2. Based on the system of fuel damage occurrence in BWRs or PWRs, restrictions at normal operation and allowable limits at abnormal transient are determined in the fuel design considering the each following;

- (i) Cladding damage due to overheating resulting from insufficient cooling
- (ii) Cladding damage due to deformation resulting from a relative expansion between pellet and cladding

Table 2.2 Criteria and allowable limits of fuel damage in BWR and PWR

Damage		BWR	PWR
(i) Cladding overheating	Criteria	The fuel cladding integrity ensures that during normal operation and abnormal transients, at least 99.9 % of the fuel rods in the core do not experience transition boiling	The DNB design basis requires at least a 95 % probability, at a 95 % confidence level, that the limiting fuel rods in the core will not experience DNB during normal operation or any transient conditions
	Allowable limits at transient	MCPR: 1.07	MDNBR: 1.30
	Restrictions at normal	MCPR: 1.2–1.3	MDNBR: 1.72
(ii) Cladding deformation	Criteria	The fuel cladding integrity ensures that during normal operation and abnormal transients, the fuel rods in the core do not experience circumferential plastic deformation over 1 % by PCI	The fuel cladding integrity ensures that during normal operation and abnormal transients, the fuel rods in the core do not experience circumferential deformation (elastic, plastic, and creep) over 1 % by PCI
	Allowable limits at transient	Direct evaluation of criteria by experiments	MLHGR: 59.1 kW/m (2,300 °C fuel centerline temperature)
	Restrictions at normal	MLHGR: 44 kW/m	MLHGR: 43.1 kW/m (1,870 °C fuel centerline temperature)

For damage mechanism (i), the BWR criterion is that “the fuel cladding integrity ensures that during normal operation and abnormal transients, at least 99.9 % of the fuel rods in the core do not experience transition boiling”. In PWRs, similarly, the criterion is that “the DNB design basis requires at least a 95 % probability, at a 95 % confidence level, that the limiting fuel rods in the core will not experience DNB during normal operation or any transient conditions”. (DNB means the departure from nucleate boiling.)

Based on those criteria, the BWR design requires the allowable limit of the minimum critical power ratio (MCPR) to be 1.07 at abnormal transients and the restriction to be 1.2–1.3 at normal operation. Similarly, the PWR design has the allowable limit of minimum heat flux ratio (minimum departure from nucleate boiling ratio, MDNBR) to be 1.30 at abnormal transients and the restriction to be 1.72 at normal operation.

For the damage mechanism (ii), the BWR criterion is that “During normal operation and abnormal transients, the fuel rods in the core do not experience circumferential plastic deformation over 1 % by PCI”. In PWRs, similarly, the criterion is that “During normal operation and abnormal transients, the fuel rods

Table 2.3 Fuel rod behavior in FEMAXI-6

	Thermal behavior (temperature dependent)	Mechanical behavior
Pellet	Thermal conduction (radial heat flux distribution) Fission gas release (temperature and burnup dependent)	Thermal expansion, elasticity and plasticity, creep, cracking, initial relocation, densification, swelling (solid FPs and gas bubbles), hot-press
Cladding	Thermal conduction Oxidation film growth	Thermal expansion, elasticity and plasticity, creep, irradiation growth, oxidation film growth
Fuel Rod	Gap thermal conduction (mixed gas, contact, radiation) Cladding surface heat transfer Gap gas flow	PCMI (pellet cladding mechanical interaction), friction, bonding

in the core do not experience circumferential deformation (elastic, plastic, and creep) over 1 % by PCI”.

Central melting of pellets in LWR fuel causes a phase change and a volume increase, and the fuel cladding may be substantially deformed mainly due to pellet cladding mechanical interaction (PCMI). The fuel rod design criteria of PWRs require that the fuel centerline temperature will be lower than the pellet melting point. Hence, the allowable limit of the fuel centerline temperature is determined to be 2,300 °C at abnormal transients and its corresponding maximum linear power density is 59.1 kW/m. The restrictions at normal operation are 1,870 °C for the fuel centerline temperature and 43.1 kW/m of the maximum linear power density.

For internal pressure of fuel rods, the BWR design requires that the cladding stress due to the internal pressure will be less than the allowable strength limit. The PWR design restricts the internal pressure of fuel rods to less than the rated pressure of primary coolant (157 kg/cm²-g) in order to avoid expansion of the gap between pellet and cladding due to creep deformation of cladding outside at normal operation. This phenomenon is called “lift-off”. The criteria of “ASME B&PV Code Sec III” are used as allowable stress limits for LWRs.

[2] Fuel rod behavior calculation

The fuel rod behavior caused by irradiation of fuel pellets and cladding is complicated for investigation in an analytical method. Fuel rod behavior calculation codes were developed from various experiments and operational experiences. FEMAXI-6 [30] as an open code developed in Japan is a general analysis code for fuel rod behavior at normal operation or abnormal transients in LWRs. It constructs a model composed of one fuel pellet, cladding, and internal gas, and then analyzes thermal, mechanical, and chemical behavior and reciprocal action at normal operation or abnormal transients from overall power history data. Table 2.3 shows fuel rod behavior analyzed in FEMAXI-6.

The overall structure of FEMAXI-6 consists of two parts, thermal analysis and mechanical analysis, as shown in Fig. 2.49. The thermal analysis part evaluates radial and axial temperature distributions considering a change in gap size between pellet and cladding, FP gas release models, axial gas flow and

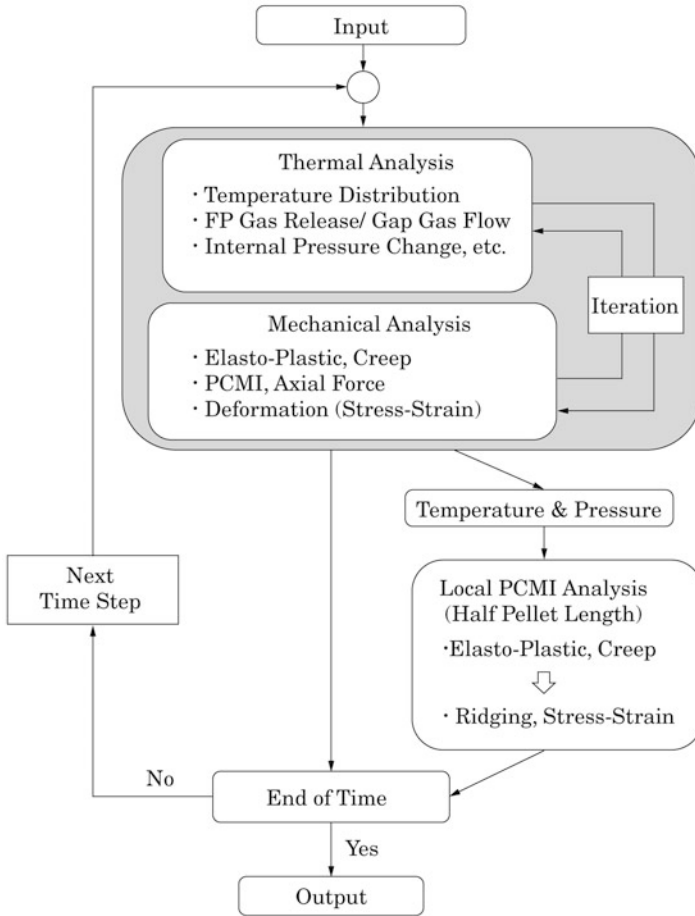


Fig. 2.49 Overview of FEMAXI-6 structure

its feedback to heat transfer in gap, and so on. The mechanical analysis part applies the finite element method (FEM) to the whole fuel rod and analyzes mechanical behavior of fuel pellet and cladding as well as PCMI. It also calculates an initial deformation due to thermal expansion, fuel densification, swelling, and pellet relocation, and then calculates stress and deformation of pellet and cladding considering cracking, elasticity/plasticity, and pellet creep. The thermal and mechanical analysis is iteratively performed to consider the thermal feedback effect on the fuel rod mechanical behavior. Further, the local PCMI can be analyzed by the 2D FEM, based on the calculation results from both analysis parts such as temperature distribution and internal pressure.

Figure 2.50 describes the calculation model of FEMAXI-6. The entire fuel rod is divided axially into several tens of segments and radially into ring elements. For example, the figure shows ten axial and radial divisions in the fuel pellet.

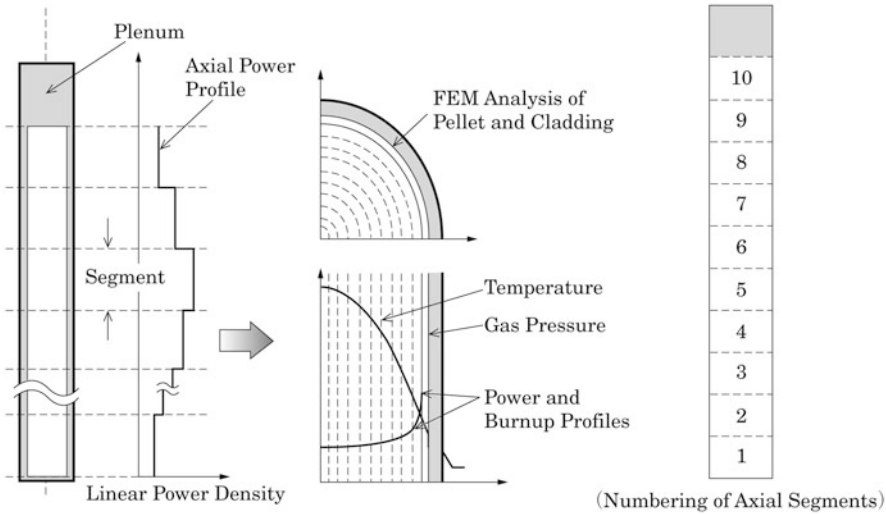


Fig. 2.50 FEMAXI-6 calculation model

FEMAXI-6 contains various calculation models and experimental correlations that users can specify. Details of models, physical properties, or correlations are described in the code manual [30] of FEMAXI-6.

Exercises of Chapter 2

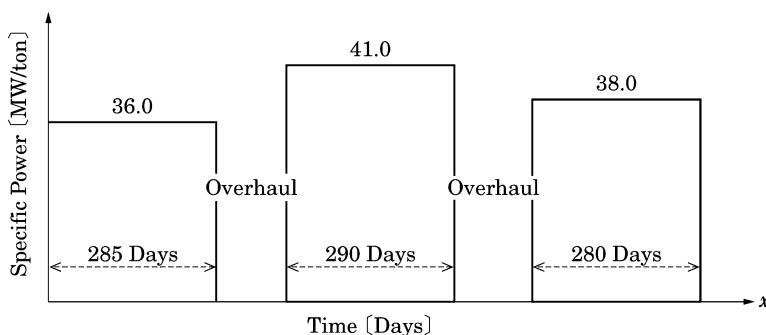
- [1] Consider a PWR UO_2 pellet 0.81 cm in diameter, 1.0 cm in height, and 10.4 g/cm^3 in density in which the uranium is enriched to 3.2 wt. % ^{235}U . Answer the following questions.
- (a) Calculate the atomic number densities of ^{235}U , ^{238}U , and O in the pellet. UO_2 contains only ^{235}U , ^{238}U , and O. Their atomic masses are $M(^{235}\text{U}) = 235.04$, $M(^{238}\text{U}) = 238.05$, and $M(\text{O}) = 16.0$, and Avogadro's number is 0.6022×10^{24} .
- (b) One-group microscopic cross sections of ^{235}U , ^{238}U , and O are given in the following table.

Nuclide	Absorption σ_a (barn)	Fission σ_f (barn)
^{235}U	50	41
^{238}U	1.00	0.10
O	0.0025	0.00

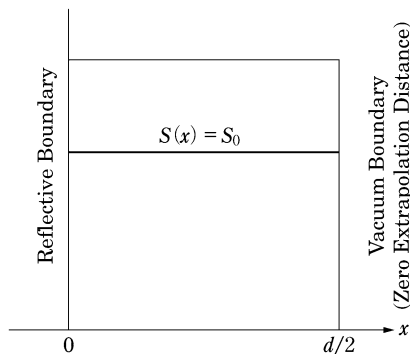
(1 barn = 10^{-24} cm^2)

Compute the macroscopic absorption and fission cross sections of the pellet. What is the probability that a neutron will cause a fission on being absorbed into the pellet?

- (c) Compute the mass (in tons) of metal uranium in one pellet 1.0 cm in height. A PWR fuel assembly consists of 265 fuel rods bundled into a 17×17 array (including 24 guide tubes) with an active height of 366 cm. Compute the initial mass of uranium in one fuel assembly and compute the total loading amount of uranium (the mass of metal uranium) in the core which contains the 193 fuel assemblies.
- (d) Calculate the linear power density (W/cm) of the fuel rod when one-group neutron flux in the pellet is 3.2×10^{14} n/cm²-s. The energy released per fission is 200 MeV ($1 \text{ MeV} = 1.602 \times 10^{-13} \text{ J}$). What is the specific power [power per initial mass of metal uranium (MW/ton)]?
- (e) Compute the burnup (MWd/ton) of the pellet consumed along the specific powers as shown in the figure



- (f) Compute the consumed amount of ^{235}U in the pellet from the burnup of (e). Two-thirds of the total power is generated by the uranium (^{235}U and ^{238}U) fission and the rest by the fission of plutonium produced from the conversion of ^{238}U .
- [2] An infinite slab of non-multiplying uniform medium of thickness d ($= 400 \text{ cm}$) contains a uniformly distributed neutron source S_0 as shown in the following figure.



The neutron flux distribution in the slab can be determined by solving the one-group diffusion equation

$$-D \frac{d^2 \phi(x)}{dx^2} + \Sigma_a \phi(x) = S_0$$

where $D = 1.0$ cm, $\Sigma_a = 2.5 \times 10^{-4}$ cm $^{-1}$, and $S_0 = 1.0 \times 10^{-3}$ n/cm 2 -s. Discretize one side to the reflective boundary in the middle into four meshes ($N = 4$) and calculate the neutron flux distribution using the finite difference method. Plot the distribution and compare it with the analytical solution

$$\phi(x) = \frac{S_0}{\Sigma_a} \left(1 - \frac{\cosh\left(\frac{x}{L}\right)}{\cosh\left(\frac{d}{2L}\right)} \right) \quad \text{where, } L = \sqrt{D/\Sigma_a}$$

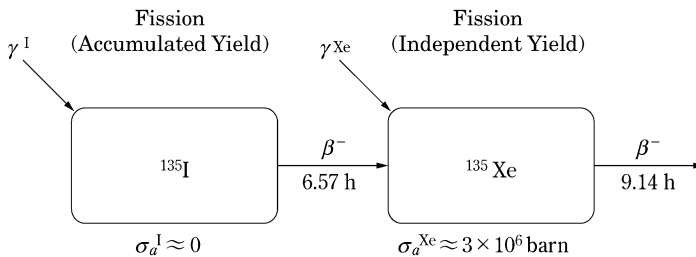
Calculate for $N = 8$ and 16 if programming is available.

- [3] (a) Consider a multiplying system with an effective multiplication factor k_{eff} . Develop the diffusion equations for fast and thermal groups in terms of the two-group constant symbols in the following table.

Fast group		Thermal group	
χ_1	1.00	χ_2	0.00
ν_1	2.55	ν_2	2.44
$\Sigma_{f,1}$	2.76×10^{-3}	$\Sigma_{f,2}$	5.45×10^{-2}
$\Sigma_{a,1}$	9.89×10^{-3}	$\Sigma_{a,2}$	8.20×10^{-2}
$\Sigma_{1 \rightarrow 2}$	1.97×10^{-2}	$\Sigma_{2 \rightarrow 1}$	0.00
D_1	1.42	D_2	0.483

- (b) Calculate the infinite multiplication factor k_∞ using the two-group constants.

- [4] The burnup chain of ^{135}I and ^{135}Xe is given by the following figure

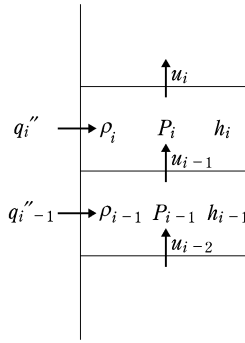


Show that the equilibrium concentration of ^{135}Xe (N_∞^{Xe}) in the reactor operating at a sufficiently high neutron flux is given approximately by

$$N_{\infty}^{\text{Xe}} = \frac{(\gamma^{\text{I}} + \gamma^{\text{Xe}}) \Sigma_f}{\sigma_a^{\text{Xe}}}$$

where γ^{I} and γ^{Xe} are the fission yields of ^{135}I and ^{135}Xe respectively, and σ_a^{Xe} is the one-group microscopic absorption cross section of ^{135}Xe and Σ_f is the one-group macroscopic fission cross section.

- [5] The energy conservation equation is given by Eq. (2.117) for no water moderation rod. Develop the energy conservation equation when introducing the water moderation rod.
- [6] Develop equations for single-phase transient analysis at the 1D axial node i of a single coolant channel, based on the mass conservation equation [Eq. (2.116)], the energy conservation equation [Eq. (2.117)], the momentum conservation equation [Eq. (2.118)], and the state equation [Eq. (2.119)], referring to the figure.



References

1. Lamarsh JR (1966) Introduction to Nuclear Reactor Theory. Addison-Wesley, Reading
2. Shibata K et al (2011) JENDL-4.0: a new library for nuclear science and engineering. J Nucl Sci Tech 48:1
3. Chadwick MB et al (2011) ENDF/B-VII.1 nuclear data for science and technology: cross sections, covariances, fission product yields and decay data. Nucl Data Sheets 112:2887
4. Koning A et al (ed) (2006) The JEFF-3.1 nuclear data library. JEFF report 21, NEA Data Bank
5. Trkov A, Herman M, Brown DA (eds) (2012) ENDF-6 Formats manual, data formats and procedures for the evaluated nuclear data files ENDF/B-VI and ENDF/B-VII. CSEWG Document ENDF-102, BNL-90365-2009 Rev. 2
6. Kobayashi K (1996) Nuclear reactor physics. Korona Press, Tokyo (in Japanese)
7. Okumura K, Kugo T, Kaneko K, Tsuchihashi K (2007) SRAC2006: a comprehensive neutronics calculation code system, JAEA-Data/Code 2007-004. Japan Atomic Energy Agency, Tokai-mura
8. Hazama T, Chiba G, Sato W, Numata K (2009) SLAROM-UF: ultra fine group cell calculation code, JAEA-Review 2009-003. Japan Atomic Energy Agency, Tokai-mura
9. MacFarlane RE, Kahler AC (2010) Methods for processing ENDF/B-VII with NJOY. Nucl Data Sheets 111:2739
10. Cullen DE (2012) PREPRO 2012 ENDF/B pre-processing codes, IAEA-NDS-39. IAEA Nuclear Data Section, Vienna

11. X-5 Monte Carlo Team (2003) MCNP: a general Monte Carlo N-particle transport code, version 5, LA-UR-03-1987
12. Nagaya Y, Okumura K, Mori T, Nakagawa M (2005) MVP/GMVP II: general purpose Monte Carlo codes for neutron and photon transport calculations based on continuous energy and multigroup methods. JAERI 1348. Japan Atomic Energy Research Institute, Tokai-mura
13. Knott D, Yamamoto A (2010) Lattice physics computation. In: Handbook of nuclear engineering, vol 2. Springer, New York, p 913
14. Nuclear Handbook Editorial Committee (2007) Nuclear handbook. Ohmsha Press, Tokyo (in Japanese)
15. Okumura K (2007) COREBN: a core burn-up calculation module for SRAC2006, JAEA-Data/Code 2007-003. Japan Atomic Energy Agency, Tokai-mura
16. Tasaka K (1997) DCHAIN: code for analysis of build-up and decay of nuclides, JAERI 1250. Japan Atomic Energy Research Institute, Tokai-mura (in Japanese)
17. Croff AG (1983) ORIGEN2: a versatile computer code for calculating the nuclide compositions and characteristics of nuclear materials. Nucl Tech 62:335
18. Lawrence RD (1986) Progress in nodal methods for the solution of the neutron diffusion and transport equations. Prog Nucl Energy 17(3):271
19. Expert Research Committee on Improvement in Neutronics Calculation (2001) Status and prospect of improvement in neutronics calculation. Atomic Energy Society of Japan, Tokyo (in Japanese)
20. Greenman G, Smith KS, Henry AF (1979) Recent advances in an analytic nodal method for static and transient reactor analysis. In: Proceedings of the computational methods in nuclear engineering. ANS, Williamsburg, VA, pp 3–49, 23–25 Apr 1979
21. Okumura K (1998) MOSRA-light: high speed three-dimensional nodal diffusion code for vector computers, JAEA-Data/Code 98-025. Japan Atomic Energy Research Institute, Tokai-mura (in Japanese)
22. Ito N, Takeda T (1990) Three-dimensional multigroup diffusion code ANDEX based on nodal method for cartesian geometry. J Nucl Sci Tech 27:350
23. Iwamoto T, Yamamoto M (1999) Advanced nodal methods of the few-group BWR core simulator NEREUS. J Nucl Sci Tech 36:996
24. Argonne Code Center (1977) Benchmark problem book (11. Multi-dimensional (x-y-z) LWR model), ANL-7416, Suppl. 2. Argonne National Laboratory, Illinois
25. Yamaji A (2005) Core and fuel design of the super LWR. Ph.D. Thesis, University of Tokyo (in Japanese)
26. Oka Y et al (2009) Nuclear plant engineering, section 6–2: supercritical water-cooled reactor. Ohmsha Press, Tokyo (in Japanese)
27. Oka Y, Koshizuka S, Ishiwatari Y, Yamaji A (2010) Super light water reactor and super fast reactor. Springer, New York
28. Yi TT (2004) Startup and stability of a high temperature supercritical-pressure light water reactor. Ph.D. Thesis, University of Tokyo
29. Ishiwatari Y (2006) Safety of the super LWR. Ph.D. Thesis, University of Tokyo (in Japanese)
30. Suzuki M, Saitou H (2006) Light water reactor fuel analysis code FEMAXI-6(Ver.1) – Detailed Structure and User’s Manual JAEA-Data/Code 2005-003). Japan Atomic Energy Agency, Tokai-mura
31. Oka Y, Suzuki K (2008) Nuclear reactor dynamics and plant control. Ohmsha Press, Tokyo (in Japanese)
32. The Japan Society of Mechanical Engineers (1986) Heat transfer, Rev. 4. The Japan Society of Mechanical Engineers (in Japanese)

Nuclear Reactor Design

Oka, Y. (Ed.)

2014, XIII, 327 p. 190 illus., 1 illus. in color., Hardcover

ISBN: 978-4-431-54897-3